We are IntechOpen,
the world's leading publisher of
Open Access books
Built by scientists, for scientists

4,800
Open access books available

122,000
International authors and editors

135M
Downloads

Our authors are among the

154
Countries delivered to

TOP 1%
most cited scientists

12.2%
Contributors from top 500 universities

BOOK CITATION INDEX
CLARIVATE ANALYTICS
INDEXED

WEB OF SCIENCE™

Selection of our books indexed in the Book Citation Index
in Web of Science™ Core Collection (BKCI)

Interested in publishing with us?
Contact book.department@intechopen.com

Numbers displayed above are based on latest data collected.
For more information visit www.intechopen.com

Design and Development of Two-Dimensional Strained Layer Superlattice (SLS) Detector Arrays for IR Applications

Ashok K. Sood, John W. Zeller, Roger E. Welser,
Yash R. Puri, Nibir K. Dhar,
Priyalal S. Wijewarnasuriya and Sanjay Krishna

Additional information is available at the end of the chapter

Abstract

The implementation of strained layer superlattices (SLS) for detection of infrared (IR) radiation has enabled compact, high performance IR detectors and two-dimensional focal plane arrays (FPAs). Since initially proposed three decades ago, SLS detectors exploiting type II band structures existing in the InAs/GaSb material system have become integral components in high resolution thermal detection and imaging systems. The extensive technological progress occurring in this area is attributed in part to the band structure flexibility offered by the nearly lattice-matched InAs/AlSb/Ga(In)Sb material system, enabling the operating IR wavelength range to be tailored through adjustment of the constituent strained layer compositions and/or thicknesses. This has led to the development of many advanced type II SLS device concepts and architectures for low-noise detectors and FPAs operating from the short-wavelength infrared (SWIR) to very long-wavelength infrared (VLWIR) bands. These include double heterostructures and unipolar-barrier structures such as graded-gap M-, W-, and N-structures, nBn, pMp, and pBn detectors, and complementary barrier infrared detector (CBIRD) and pBiBn designs. These diverse type II SLS detector architectures have provided researchers with expanded capabilities to optimize detector and FPA performance to further benefit a broad range of electro-optical/IR applications.

Keywords: strained layer superlattice, infrared sensors, focal plane array, thermal imaging, type II

1. Introduction

Infrared (IR) sensors have been and continue to be developed for a variety of commercial and military systems applications, which include short-wavelength infrared (SWIR), mid-wavelength infrared (MWIR), long-wavelength infrared (LWIR), and very long-wavelength infrared (VLWIR) detectors [1]. Conventional SWIR detectors operate over the ~0.9–2.5 μm region above the visible band [2]. MWIR sensors sensitive in the 3–5 μm region have typically been based on InSb or HgCdTe (MCT) [3]. In addition, LWIR and VLWIR sensors for 8–12 μm applications commonly utilize MCT or microbolometer technology [4]. Quantum well infrared photodetectors (QWIPs) are another relatively recent IR sensing technology, which can be designed to operate over the MWIR to VLWIR range.

While large format III–V InSb focal plane arrays (FPAs) have been developed, the fixed bandgap of InSb detectors restricts their operation to the MWIR, and such devices are limited to cryogenic temperatures [5, 6]. MCT detectors are known for high quantum efficiencies (above 90%) and detectivities, but require expensive and relatively scarce CdZnTe substrates for optimal performance, and nonuniform growth defects are a substantial limiting factor for MCT-based FPAs [7]. In addition, performance limitations of inexpensive microbolometers, particularly in relation to sensitivity and speed, are well-known [8].

Since their initial development, IR photodetectors based on strained layer superlattices have drawn much interest from research and commercial sectors in recent decades. SLS detectors typically exploit type II band structures existing in InAs/GaSb, which constitutes an attractive material system for developing MWIR and LWIR detectors with advanced properties. As illustrated in **Figure 1(a)** [9], type II superlattices are characterized by a staggered band alignment in which the conduction band of the InAs layer is lower than the valence band of the InGaSb layer [10]. The implementation of barrier layers in the photoconductor structure in type II SLS detectors prevents current flow of minority and/or majority carriers, leading to higher performance antimonide-based FPAs [11]. In such structures, varying the thickness of the InAs layers can have a substantial impact on the spectral response (**Figure 1(b)**) [9].
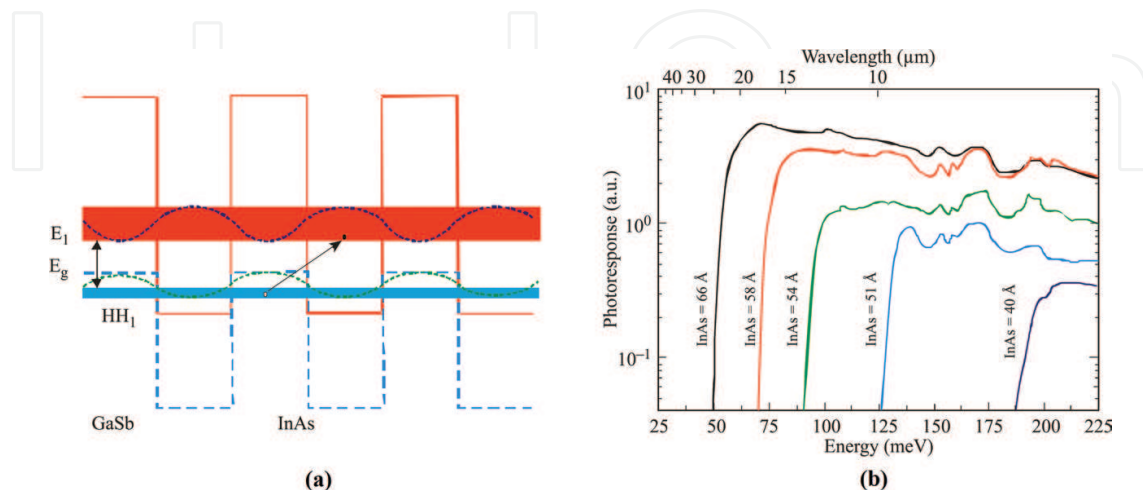

Figure 1. Band edge diagram of InAs/GaSb SLS, illustrating the confined electron and hole minibands which form the energy bandgap; and (b) charted change in cutoff wavelength with InAs thickness for fixed GaSb thickness of 40 Å in type II SLS detector [9].

In the nearly lattice-matched InAs/AlSb/Ga(In)Sb 6.1 Å family material system, type I (nested, or straddling), type II staggered, and type II broken-gap (misaligned, or type III) energy-band alignments are all realizable [8]. The 6.1 Å family material includes wide, medium, and narrow gap components, with GaSb, insulating AlSb, and high mobility InAs (see **Figure 2**) [12, 13]. Type II InAs/GaSb SLS detectors offer broad design band structure flexibility: it is possible in these materials to tailor the IR operating wavelength from 3 μm to around 30 μm, covering most of the practical IR wavelength spectrum [14]. For example, the effective band-gap (and corresponding detection wavelength) of an InAs/Ga(In)Sb type II SLS can be varied continuously (theoretically in the range of 0 to about 400 meV) by changing the thicknesses of constituent layers and/or ternary compound composition [11]. Since the electron-hole overlap in such detectors is controlled by the thicknesses of the constituent layers, it is possible to fabricate small bandgap materials using "mid-gap" semiconductors.

The strain within the superlattice (SL) layers in type II SLS detectors create a large splitting between the heavy-hole and light-hole bands in the ternary superlattices [15]. This reduces the hole-hole Auger recombination process and increases the minority carrier lifetime, thereby improving the device detectivity (D^*) and lowering the required operating temperature [16]. By optimizing the oscillator strength in this material system, a large quantum efficiency and responsivity can likewise be obtained [17]. In addition, type II SLS detectors based on the 6.1 Å family of materials can be passively cooled, thus reducing the cryocooler burden, and these take advantage of the relatively large installed III–V material manufacturing base [18]. These properties have enabled the fabrication of large format IR FPAs based on type II SLS suitable for high-resolution thermal imaging applications including space-borne surveillance systems, low-background night vision, and missile detection [19–26].

InAs/GaSb in type II SLS is the only known type of IR detector material having theoretically higher performance than precedential HgCdTe (MCT), due primarily to longer Auger life-times [28]. Also, the larger effective mass in InAs/Ga(In)Sb leads to a reduction of tunneling currents in type II SLS detectors compared with MCT detectors of the same bandgap, while high electron mobility and diffusivity is maintained [29, 30]. In addition, III–V materials offer
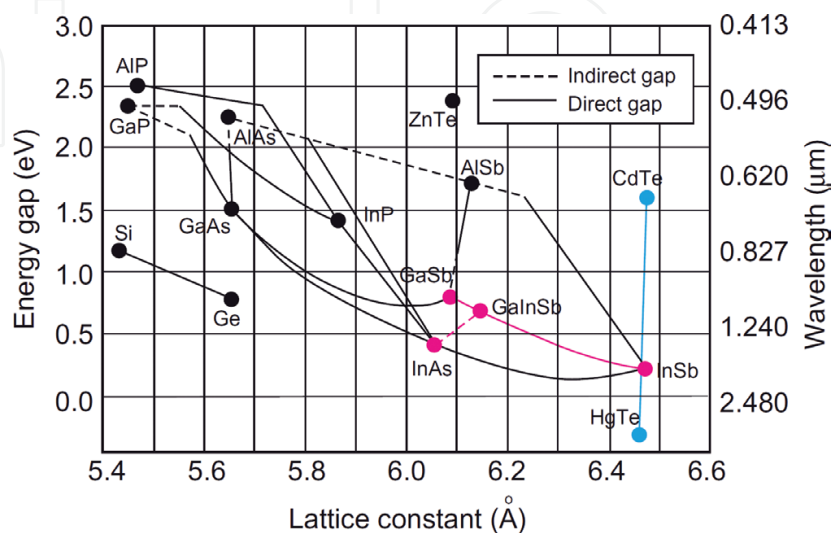

Figure 2. Compositional and wavelength/energy gap dependence diagram of antimonide-based III–V material systems [12].

much stronger chemical bonds compared to MCT, potentially providing higher chemical stability and thus better producibility [8]. Furthermore, SLS detectors can detect normal incident IR radiation, in contrast to *n*-type QWIPs that are thus prevented due to polarization selection rules of intersubband transitions that limit quantum efficiencies to 10–20% [31]. These features, combined with the suppression of Auger recombination due in part to the decoupled spin-orbital splitting with SL bandgap, make InAs/Ga(In)Sb SLS a very competitive material system for next generation IR detectors and FPA technologies. **Figure 3** presents a comparison of thermal detectivities versus temperature calculated for various detector technologies, including SLS, HCT, and QWIP [27].

The existence of type II staggered energy band alignments in the 6.1 Å material family allow the development of many advanced heterojunction device concepts and architectures for reduced noise IR SLS detectors, one of which is shown in **Figure 4** [11]. These include graded-gap W- [19], M- [20], and N-structures [32]; buried junction nBn [21], pBp [22], and pBn [33] designs; and complementary barrier infrared detector (CBIRD) [23] and pBiBn [24] architectures. These device implementations are the result of exploitation of the material, electrical, and optical properties in type II SL materials for optimization of detector performance, which can benefit and advance a diverse array of applications.

This chapter will cover the development of type II superlattice materials and detector device architectures for next generation IR FPA technologies, primarily for MWIR and longer wavelength applications. Section 2 discusses the progress and achievements of type II SL-based technological development up to the present. This includes the historical development of detector architectures for low-noise IR detection and their noteworthy performance features, as well as a discussion of the nature and relevance of the different IR bands to SLS detectors and FPAs. Section 3 presents a theoretical analysis of noise components common to SLS detectors and their respective impact on design considerations and performance. Section 4 focuses on the compositions, features, and benefits of the various optimized type II SLS detector architectures developed. In particular, relevant aspects among individual dark current
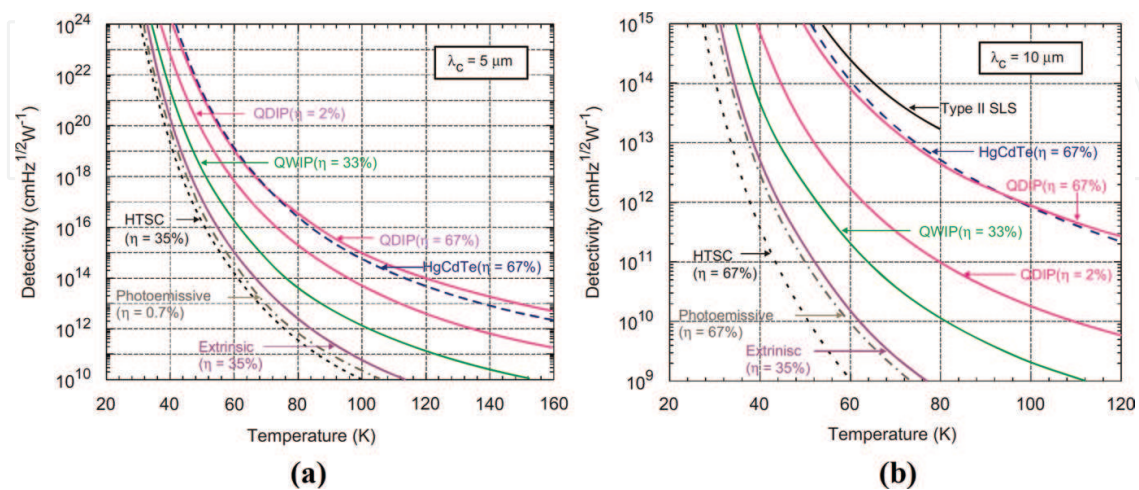
Figure 3. Calculated thermal detectivity as function of temperature for various MWIR (λ_c = 5 μm) (a) and LWIR (λ_c = 10 μm) (b) photodetectors, where predicted quantum efficiencies are indicated [27].
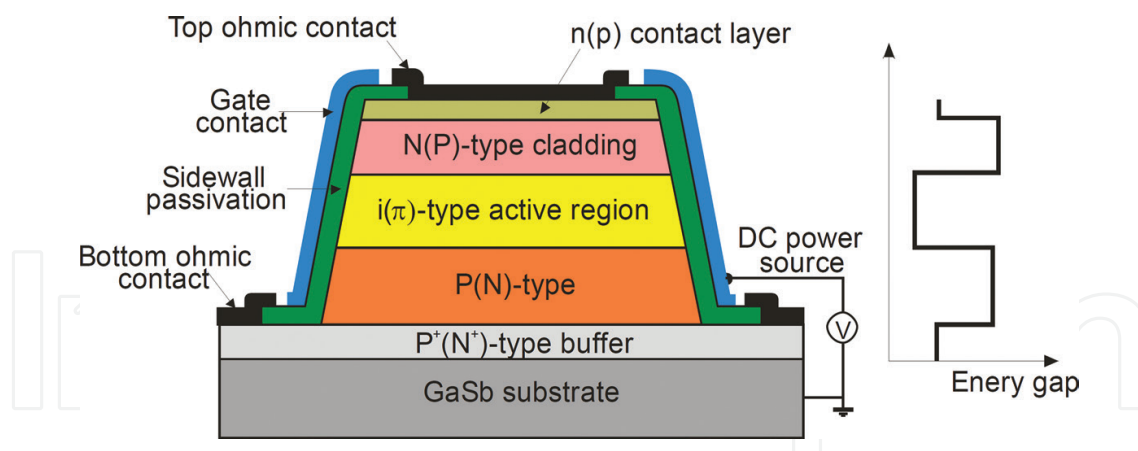
Figure 4. Schematic band diagram of *n-i-p* double heterostructure antimonide-based III–V photodiode [11].

mechanisms with respect to the material quality, operating conditions, and performance of the type II SLS detector structures will be addressed. Finally, in Section 5, notable trends and practical progress made in the development of type II SLS detectors and FPAs are discussed that have had and/or are expected to have a significant impact on the status of IR sensing and imaging technology.

2. Technological development of type II SLS detectors

2.1. Historical development of SLS detectors

2.1.1. Development of type II SLS detectors

The developmental timeline of type II SLS detector technology commenced in the 1970s when investigations were carried out, most notably by Esaki and Tsu, of near lattice-matched InAs/GaSb superlattices systems as alternatives to GaAs/AlGaAs superlattices [34]. The first fundamental superlattices structure, based on InAsSb/InAsSb and capable of achieving small infrared energy gaps with strong interactions between them, was reported in 1977 by Sai-Halasz et al. [35]. A decade later, in 1987, Smith and Mailhiot proposed an InAsSb/InSb type II SLS for IR detection applications, which was predicted theoretically to provide favorable optical properties including small diode tunneling currents and good mobilities and diffusion lengths [36]. By 1997, the device material quality had been greatly improved and band-to-band (BTB) tunneling currents suppressed, enabling fabrication of devices using the molecular beam epitaxy (MBE) process. One early MWIR SLS detector device developed around this time demonstrated a responsivity of 2 A/W, as well as Johnson noise-limited detectivity in excess of 10^{12} cm√Hz/W, or Jones [37].

In 2007, Rodriguez et al. demonstrated the first type II SLS nBn detector that was capable of performing up to 300 K due to reduction of both Shockley-Read-Hall (SRH) generation currents and surface recombination currents [7]. The pBiBn design (LWIR) was first introduced in 2010 by Gautam et al., which due to its unipolar blocking layers exhibited comparatively low

(at the time) dark current density of 1.2 mA/cm² [24], and in 2012 this group demonstrated MWIR pBiBn detectors capable room temperature operation [38]. That same year DeCuir et al. reported a type II SLS pBiBn structure with 50% cutoff wavelength of 8.7 μm that demonstrated low dark current density of ~10 μA/cm² at −50 mV [39].

By 2014, LWIR nBn photodetectors had been developed demonstrating peak responsivity of ~4.5 A/W at 7.9 μm, corresponding to a quantum efficiency of 54%, though the dark current density (e.g., 440 μA/cm² at 77 K) was considerably higher than that for pBiBn structure devices [43]. **Figure 5(a)** and **(b)** compare the dark current performance of type II SLS detectors from various groups with a "Rule 07" model providing a theoretical prediction of MCT detector performance as a function of wavelength and over time, respectively [7, 110, 40–42]. Likewise, **Figure 6(a)** and **(b)** chart the carrier lifetimes at 77 K for HgCdTe and type II SLS detectors operating at MWIR and LWIR wavelengths, respectively, as a function of doping concentration [11].

2.1.2. Development of type II SLS FPAs

The development of type II SLS FPAs brought a degree of practical utility that had not previously been realized to SLS device research and development. The first FPA based on type II SLS detector pixels, reported in 2002 by Cabanski et al., was a MBE-grown, 256 × 256 pixel, 40 μm pitch MWIR device that demonstrated a noise equivalent temperature difference (NETD) of under 12 mK [44]. In 2006, the first LWIR FPA based on type II SLS material was reported by Razeghi et al., which incorporated an M-structure SL design to enhance its wavelength tunability [45]. That same year a dual-band FPA was demonstrated, combining spectral selective detection in the 3.0–4.1 μm and 4.1–5.0 μm wavelength ranges at each pixel [46].
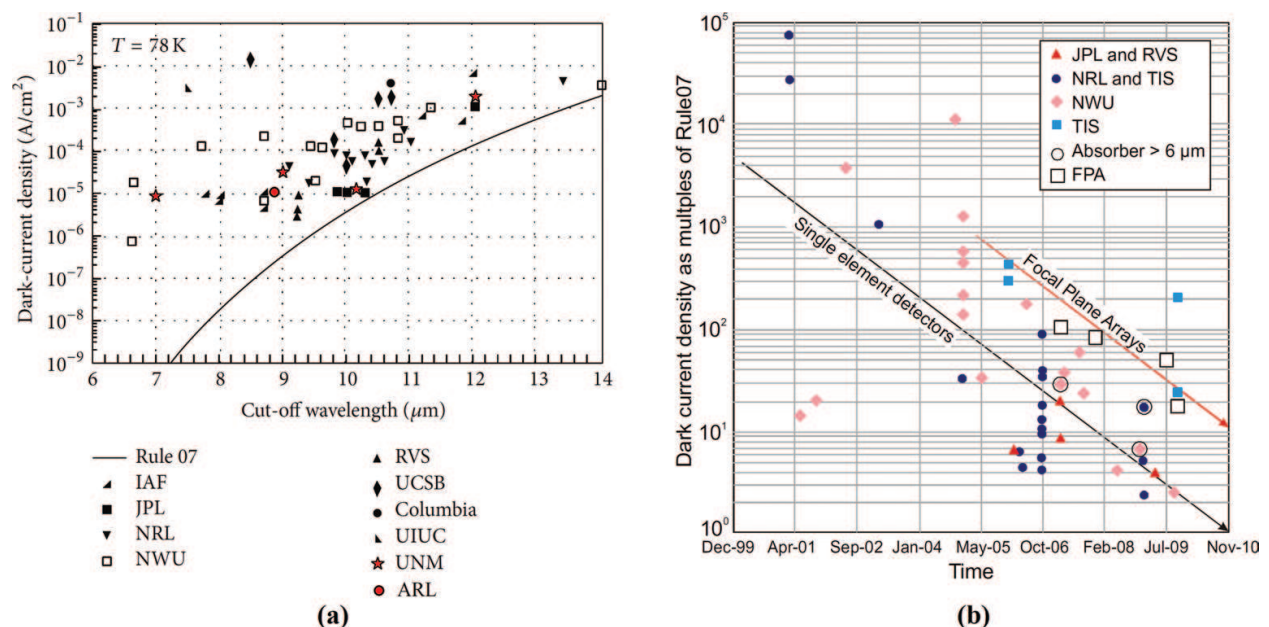
Figure 5. (a) Dark current densities plotted against cutoff wavelength for type II SLS non-barrier and barrier detectors at 78 K [7, 11]. The solid line indicates the dark current density calculated using the empirical "rule 07" model, and the circle indicates results from DeCuir et al. [39] (b) Detector dark current density as multiple of rule 07 [40–42]. The black line represents the trend line of dark current reduction over time for single element detectors, while the red line shows this trend for FPAs.
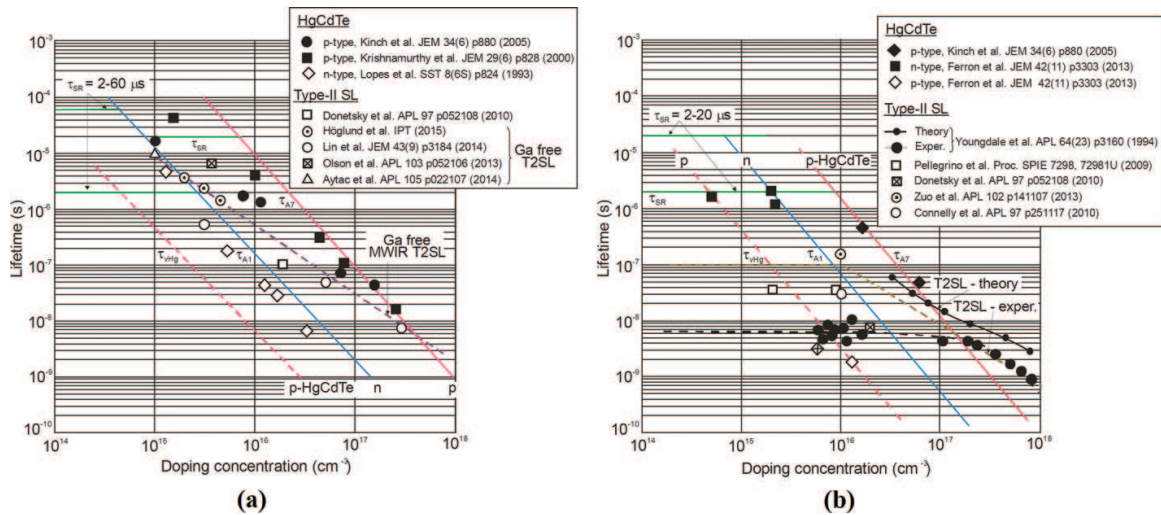
Figure 6. Carrier lifetimes for (a) HgCdTe and type II SLS MWIR detectors, and (b) HgCdTe and type II SLS LWIR detectors, at 77 K as a function of doping concentration. The dashed lines follow experimental data [11].

The first MWIR SLS FPA with megapixel (1024 × 1024) resolution was reported in 2009 by Hill et al., from which detectivities as high as 8×10^{13} Jones were measured [47]. The following year, Gunapala et al. demonstrated the first type II SLS megapixel FPA for LWIR detection, which yielded a NETD of 53 mK at 80 K [48]. From 2010 to 2012, further large format LWIR type II SLS FPAs were demonstrated; these were characterized by pixel pitches of around 20 μm and peak quantum efficiencies as high as 96% [49, 50]. In 2016, Klipstein et al. reported a 640 × 512 type II SLS LWIR FPA with pixel pitch as small as 15 μm [51]. **Figure 7(a)–(c)** show the detector pixel architecture for a recently reported type II SLS MWIR FPA featuring a *p-i-n* design, a top-view image of the detector pixel array, and a captured image from the FPA, respectively [40].

2.2. Impact of IR bands on SLS performance

2.2.1. Short-wavelength infrared (SWIR)

In contrast to the longer wavelength IR bands, the SWIR range (~0.9–2.5 μm) involves reflected light rather than thermal radiation, thus producing more visible-like images [52]. The shorter
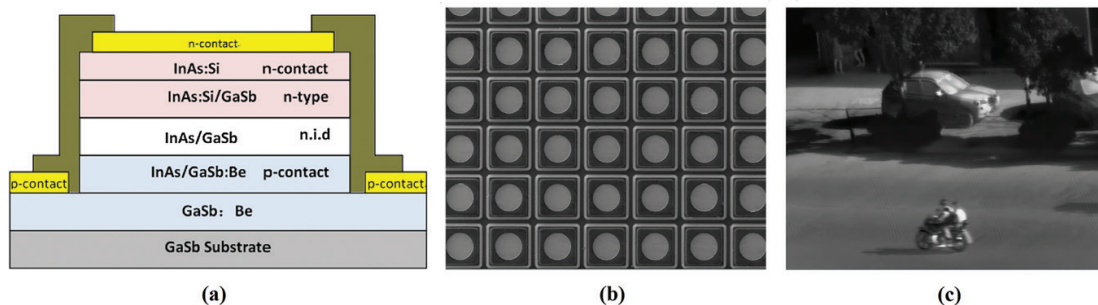
Figure 7. (a) Cross-section schematic of type II InAs/GaSb SLS MWIR FPA detector pixel. (b) Top-view SEM image of type II SLS FPA chip; and (c) outdoor image from FPA at 80 K [40].

wavelengths over this range also enable smaller SWIR FPA pixel sizes. Development of SWIR detectors based on type II SLS is comparatively challenging but has been accomplished, for example, by adding a third AlAs layer to the superlattice allowing the effective bandgap to be raised (**Figure 8**) [53], though this necessitates some degree of lattice mismatch [54]. SWIR detection has been combined on single SLS devices with both MWIR and LWIR detection capability to offer both active and passive multiband imaging [52]. SWIR detection applications include telecommunications, astronomical observation, remote sensing, spectroradiometry, spectrophotometry, and hostile mortar fire detection [53, 55].

2.2.2. Mid-wavelength infrared (MWIR)

MWIR detection involves passive imaging of electromagnetic wavelengths in the of 3–5 μm atmospheric transparent window. Rather than sensing reflected radiation as occurring at shorter wavelengths, detection of MWIR and longer wavelengths involves capturing thermal signatures, or temperature contrasts. A primary goal for MWIR detection has been to elevate the operating temperature; however, in this regard care must be taken in temperature regimes where carriers are close to the intrinsic, since at this point the thermally generated carrier concentration becomes comparable to the doping concentration [56].

The MWIR and LWIR bands are both commonly utilized for thermal IR detection, but there are significant differences between them that impact their respective detection and imaging performance. For example, the scene contrast at 300 K is 3.5–4% in the MWIR band compared to 1.7% for the LWIR band, resulting in higher attainable NETDs for the latter [57]. In addition, undesirable atmospheric water vapor effects are often present for MWIR wavelengths up to ~7.5 μm that can greatly decrease contrast at significant distances and/or in humid environments [58]. MWIR detection is utilized for many applications (a number of which are also common to LWIR), which include aerial and satellite reconnaissance, target tracking, navigation, and object identification [54].
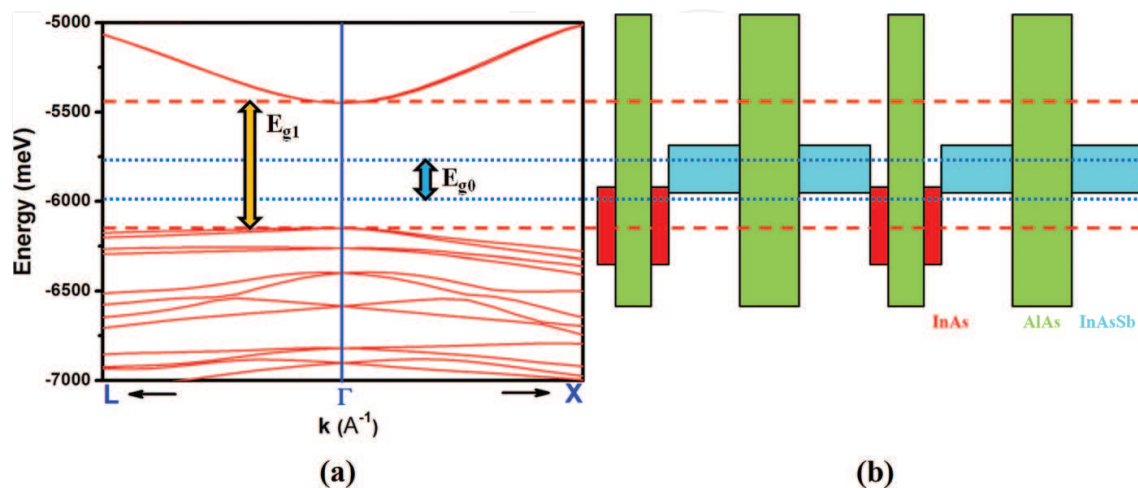
Figure 8. (a) Band structure of SWIR SLS design around C-point, where energy levels are referenced to the vacuum level. (b) Superlattice structure and formation of effective bandgap, where colored rectangles represent forbidden bandgaps of the different layers in the SL [53].

2.2.3. Long-wavelength infrared (LWIR)

The LWIR spectral band typically refers to wavelengths over the 8–14 µm range, though it can likewise be meant to describe the 8–12 µm wavelength range. LWIR detectors have traditionally incorporated relatively inexpensive microbolometer technology with low power requirements, but associated drawbacks include higher noise and lower sensitivities and speeds [8]. Based on blackbody physics, LWIR type II SL-based imaging systems offer higher temperature dynamic range and greater in-band photon radiance for a given target temperature, as well as improvements in speed, temperature range, uniformity, and stability over conventional MWIR detectors such as those based on InSb [59].

In LWIR SL-based detectors and FPAs, the decreasing energy gaps at extended IR wavelengths cause the absorbing detector materials to become more sensitive not only to bulk material properties but also to the surface states of the exposed sidewalls, so a challenge in such detectors has been to decrease the leakage current at the sidewalls of the devices in addition to the bulk dark current [54].

Since humans emit IR radiation with a peak intensity corresponding to approximately 9.2 µm, the LWIR band is best suited for applications involving observing or monitoring people in some capacity [60]. LWIR detection applications include industrial inspection, high-speed imaging, capturing high temperature targets, atmospheric absorption monitoring, and enhanced night vision [61].

2.2.4. Very long-wavelength infrared (VLWIR)

Various type II SLS detectors and FPAs have been developed capable of detection and imaging of VLWIR wavelengths (~12–30 µm) involving narrower bandgaps than for MWIR and LWIR. At present, VLWIR detector technology is dominated by MCT and extrinsic silicon blocked impurity band (BIB) detectors. Type II SLS detectors have been shown theoretically to offer better VLWIR performance above the 14 µm cutoff (beyond this issues with nonuniformity and excessive dark current arise) than MCT and BIB detectors, the latter of which require very low operating temperatures due to high thermal ionization [62, 63].

There have been considerable improvements in the optical and electrical qualities of VLWIR ternary SL materials in recent years, particularly lower Ga content, which has been achieved largely through optimization of molecular beam epitaxy (MBE) growth parameters. These have resulted in better device performance characteristics, including longer minority carrier lifetimes (e.g., ~140 ns) for VLWIR type II SLS detectors [8].

Relatively strong dark currents and low differential resistance area products (R_0A) at zero bias have limited the ability of type II SLS VLWIR FPAs to match readout integrated circuits (ROICs) for practical imaging devices [64]. Nevertheless, much progress has been made in recent years in the development of VLWIR SLS FPAs. For example, as shown **Figure 9**, a type II InAs/InAsSb VLWIR FPA grown on a GaSb substrate was reported in 2017 that produced sharp thermal images [64], and another recently that exhibited peak responsivity of 4.8 A/W and detectivity of 1.4×10^{10} Jones [65]. Potential applications of VLWIR detection and imaging include long-range ballistic missile defense, space-based astronomy, space-borne remote sensing, remote pollution monitoring, and meteorological monitoring [66, 67].
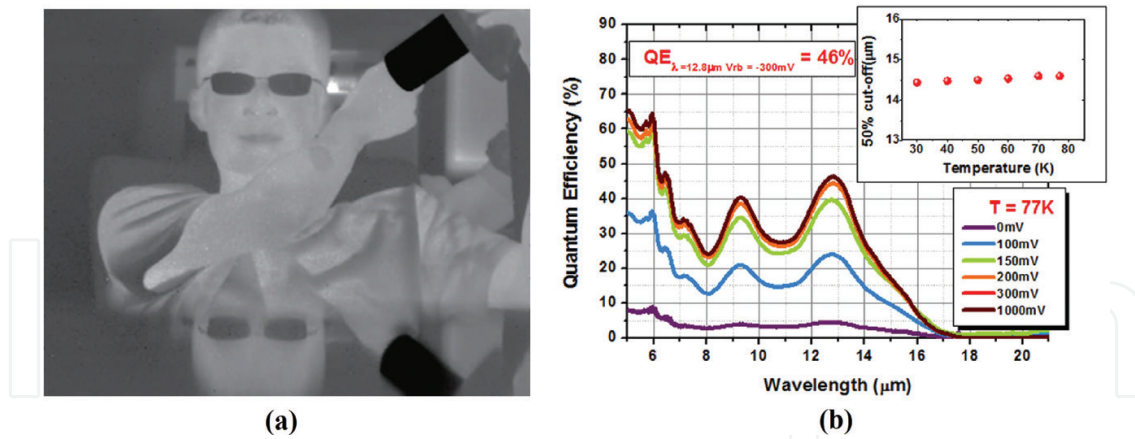
Figure 9. (a) Thermal image acquired from 320 × 256 VLWIR FPA at 65 K, in which mirror image can be seen reflected on the surface of a desk [64]. (b) Quantum efficiency spectrum with varying bias at 77 K; inset shows 50% cutoff wavelength versus temperature [65].

3. Noise contributions in SLS detectors

3.1. Impact of noise on performance

3.1.1. SLS detectors

Although InAs/Ga(In)Sb type II SLS been investigated for the past three decades, many of the fundamental material and physical properties are still not well understood. This can pose challenges in identifying the major noise mechanisms for various device architectures, which is an important step towards facilitating low-noise detector designs.

For photodetectors, dark current is basically the accumulation of current contributions from diffusion current in bulk p and n regions, generation-recombination (GR) current in the depletion region, band-to-band tunneling, trap-assisted tunneling (TAT), and surface leakage current [68]. It was discovered that the InAs/GaSb 6.1 Å material family in type II SLS detectors reduces adverse BTB/TAT currents and GR Auger contribution to the total dark current [8]. In such SLS detectors, the placement of barrier layers provides a means to effectively filter the various dark current components.

3.1.2. SLS focal plane arrays (FPAs)

Among the major issues limiting the performance of IR FPAs are charge handling capacity of the readout, residual nonuniformity of the imager, and dark current of the sensitive material [41]. The effects of dark current and its spatial variation are more prominent in LWIR imagers operating at the longer wavelength end of their operational range, and therefore even more pronounced for VLWIR. The ratio of photocurrent to dark current is another major metric, as dark current (which is very sensitive to any small detector temperature fluctuation) when high fills the wells and forces a shorter integration time, resulting in a higher temporal (background limited) NETD. Therefore, high quantum efficiency (QE) and/or faster optics for FPAs

are required if dark currents are not kept well below the photocurrent level. In **Figure 10(a)** and **(b)**, predicted dark current density and noise equivalent temperature difference (NEDT), respectively, versus temperature are compared for type II SLS and MCT detectors [57].

3.2. Major dark current contributions in SLS devices

In this section the major dark current components are discussed. We have sought to address the more relevant aspects among the individual dark current mechanisms with respect to material quality and device operation conditions.

3.2.1. Diffusion current

Diffusion current is present at any semiconductor junction, and it contributes to detector dark current under both forward and reverse bias. The diffusion current can be represented by the following equation [69]:

$$J_{diff} = n_i^2(T) \sqrt{qk_B T} \left(\frac{1}{N_A} \sqrt{\frac{\mu_e}{\tau_e}} + \frac{1}{N_D} \sqrt{\frac{\mu_h}{\tau_h}} \right) (e^{qV/k_B T} - 1) \qquad (1)$$

where $n_i(T)$ is the intrinsic carrier concentration, q is the electron charge, T is temperature, k_B is the Boltzmann constant, N_A and N_D are acceptor and donor densities, respectively, μ_e, τ_e, and μ_h, τ_h, are mobility and lifetime for electrons and holes, respectively, and V is the applied bias voltage.

The shorter lifetimes in the absorption regions of InAs/Ga(In)Sb SLS detectors compared to those in IR detectors based on alternative material systems generally result in higher diffusion dark currents. However, the diffusion current is also dependent on the doping concentration in the junction, and the doping profile may be manipulated (e.g., through *in situ* doping profile engineering during material growth) with the objective of minimizing the diffusion current.
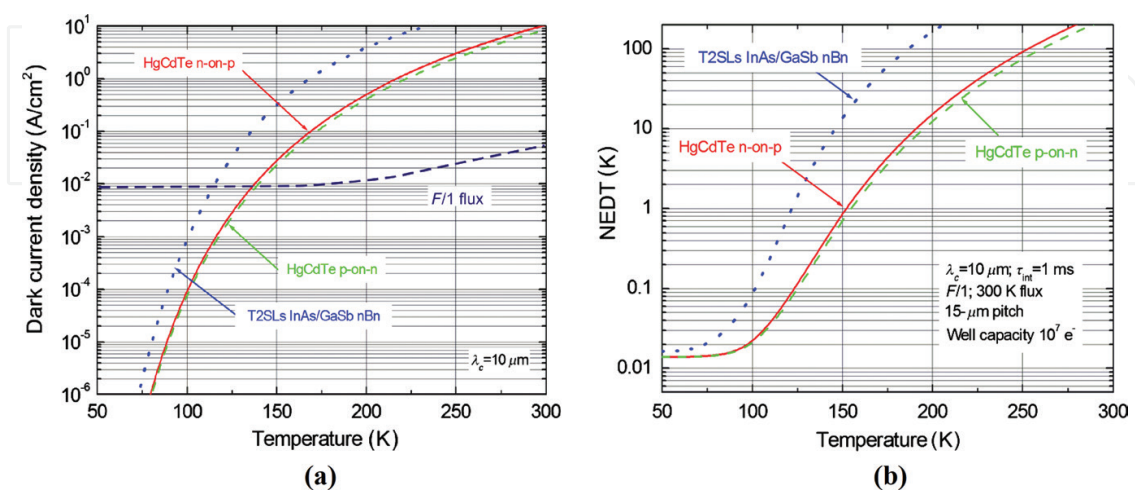
Figure 10. Calculated dark current density (a) and NETD (b) vs. temperature for HgCdTe and type II SLS InAs/GaSb nBn detectors having a cutoff wavelength (λ_c) of 10 μm [57].

3.2.2. Shockley-Read-Hall (SRH) generation-recombination (GR) current

Shockley-Read-Hall (SRH) GR dark current is mostly contributed from mid-gap defects and trap states inside semiconductor materials. These states can act as generation or recombination sites, particularly in narrow bandgap materials. In most experimental investigations performed the SRH GR current remained the major dark current component, particularly at lower operating temperatures and smaller reverse biases [38]. One means to suppress GR current is by reducing the depletion region width.

The SRH current, which is proportional to the intrinsic carrier concentration, contributes to the device noise in both bias regimes. The SRH dark current is expressed by Eq. (2) [70, 71]:

$$J_{SRH} = \frac{qn_i W}{\tau_{SRH}} \frac{2k_B T}{q(V_{bi} - V)} \sinh\left(\frac{qV}{2k_B T}\right) f(b) \tag{2}$$

$$f(b) = \int_0^\infty \frac{1}{u^2 + 2bu + 1} \quad b = e^{-qV/2k_B T} \cosh\left(\frac{E_t - E_i}{k_B T}\right)$$

where W is the depletion region width, τ_{SHR} is the generation-recombination (SRH) lifetime, V_{bi} is the built-in voltage, E_i is the intrinsic Fermi level, and E_t is the trap energy level.

It is generally believed that SRH processes are the dominating factor contributing to shorter carrier lifetimes (<100 ns) in both MWIR and LWIR type II SLS detectors [72]. For LWIR binary SLS absorbers, the rapid increase in the Auger coefficient with increasing cutoff wavelength results in short electron lifetimes that are typically in the range of 15–30 ns at 77 K, and even shorter for VLWIR [15]. SRH process statistical theory suggests the occurrence of longer carrier lifetimes in bulk InAs than in bulk GaSb material based on the respective locations of the stabilized Fermi level, from which it has been theorized that native Ga-mediated defects generated during the binary SL growth are responsible for the SRH-limited minority carrier lifetimes observed in InAs/GaSb type II SLS detectors [11].

3.2.3. Trap-assisted tunneling (TAT)

TAT current becomes the dominate current mechanism under higher electrical fields with larger values of reverse bias [38]. It occurs at or near the depletion region, where minority carriers enter a trap state from the valence band and then tunnel into the conduction band. TAT is modeled by the following Eq. [73]:

$$J_{TAT} = \frac{q^2 m_T V M^2 N_t}{8\pi \hbar^3 (E_g - E_t)} \exp\left(\frac{4\sqrt{2m_T (E_g - E_t)^2}}{3q\hbar F(V)}\right) \tag{3}$$

where m_T is the reduced tunneling effective mass, N_t is the trap density, M is the transition matrix element associated with the trap, $\hbar = h/2\pi$; h being Planck's constant, and $F(V)$ is the electric field.

In **Figure 11(a)** and **(b)**, the contributions of diffusion, GR, and TAT currents to dark current and dark current density, respectively, are plotted versus applied bias voltage [39, 74].
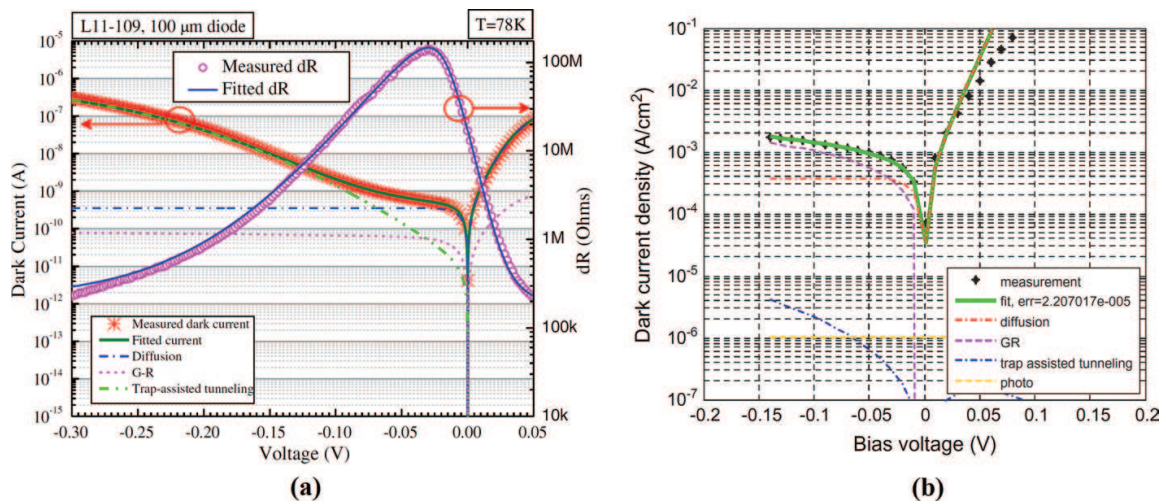
Figure 11. (a) Dark current density versus voltage for 100 μm diameter type II SLS (pBiBn) detector diode, taking into account diffusion, GR, and TAT currents. The associated differential resistance (dR) is also shown and fitted with the extrapolated dR [39]. (b) Decomposition of SLS structure device dark current at 130 K into different dark current components plotted versus bias voltage [74].

3.2.4. Band-to-band (BTB) tunneling

BTB tunneling current results from direct tunneling of carriers from the valence band into the conduction band. Like TAT, BTB is more pronounced in higher electrical field regimes and under greater reverse bias. The BTB current is also larger for higher doping levels in the active region [54].

An expression for BTB current is given by the following equation [75, 76]:

$$J_{BTB} = \frac{q^3 F(V) V}{4 \pi^2 \hbar^2} \sqrt{\frac{2 m_T}{E_g}} \exp\left(\frac{4 \sqrt{2 m_T E_g^3}}{3 q \hbar F(V)} \right) \tag{4}$$

where $F(V)$ is the electrical field under different bias voltages. Eq. (4) indicates that the tunneling dark current is strongly dependent on the bandgap, and consequently plays a more significant role in LWIR and VLWIR detectors.

3.2.5. Surface leakage current

Excessive surface leakage currents are known to limit the performance of mesa etched InAs/GaSb SL detectors, especially for LWIR detection [68]. During the FPA pixel isolation process, the periodic crystal structure can terminate abruptly, resulting in the formation of unsatisfied (dangling) chemical bonds responsible for generation of surface states within the bandgap [7]. These states cause pinning of the surface Fermi level near the mid-gap, consequently enhancing the surface leakage current [77]. Passivation, which for this purpose usually involves deposition of a relatively thick layer of dielectric material (usually SiO_2), reduces the number of surface states and is thus critical for minimizing surface leakage currents, especially in low bandgap materials [38, 78]. In SLS detectors, and in particular nBn structures, the placement and position of the barrier(s) can serve as a means to effectively reduce the surface leakage current [8].

4. Type II SLS detector design technologies

4.1. Overview

A majority of type II SLS detector structures are variations of the general double heterostructure (DH) design, such as the *p-i-n* detector device depicted in **Figure 12** with associated band structure [41, 79]. This type of structure comprises an unintentionally doped intrinsic region sandwiched between heavily doped *p* and *n* layers of larger bandgap material [11]. The DH architecture was initially intended to optimize quantum efficiency while minimizing transport barriers at the heterointerfaces [80]. It provides practical benefits over basic homojunction devices for type II SLS detectors, most notably the incorporation of current blocking layers either in the conduction or valence band that reduce multiple dark current components including GR and BTB tunneling currents.

In this section, primary classes of type II SLS detector designs are described, and in certain cases illustrated. The present classifications for the different types of SLS detectors are somewhat ambiguous in that multiple and overlapping categories exist; however, in the following discussion, attempts will be made to clarify potential conflicts. In consideration of space constraints, other less common type II SLS detectors are not covered here in detail, which include, but are not limited to, the shallow etch mesa isolation (SEMI), a type of *n*-on-*p* graded-gap "W" photodiode structure [8]; hybrid superlattice (HSL) structure [81]; and strain-compensated InAs/AlInSb superlattice barrier (ALSL-B) [82].

4.2. Buried junction

Devices generally classified as *buried junction* include nBn, pBp, and pBn architectures [6]. The pBp architecture may be considered the inverse of the nBn structure, the main distinctions being that the minority carriers for nBn are holes while those for pBp are electrons, and the barriers each differ in height relative to the valence and conduction bands [83]. These structures likewise belong to the *unipolar barrier* category, which basically describes the inclusion of a single barrier that blocks one carrier type (electron or hole) but allows for the other to flow unimpededly [79]. A unipolar barrier can be implemented either outside the depletion region in the *p*-type layer of a SLS device, or at the edge of the *n*-type absorbing layer near the
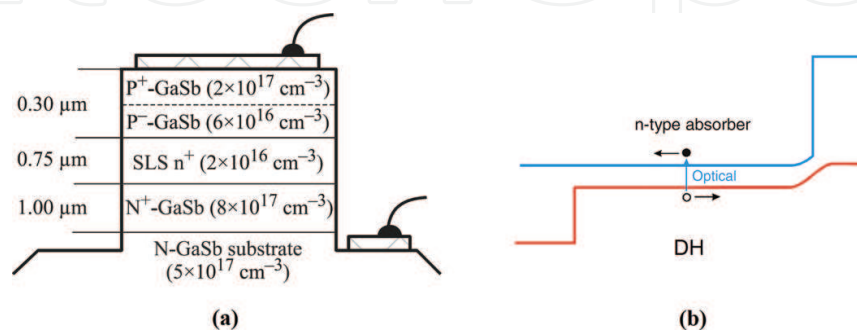
Figure 12. (a) Cross-section schematic of InAs/GaInSb SLS DH *p-i-n* detector [79]. (b) Corresponding bandgap diagram typical of DH photodiode [41].

junction [8]. To be properly implemented into a low-noise photodetector design, the unipolar carrier blocking layers must be sufficiently thick, and the conduction band offset to valence band offset ratio (CBO/VBO) large enough, to effectively block majority carriers and thereby suppress thermionic emission and direct tunneling dark current.

4.2.1. nBn design

Due to the absence of majority carrier flow, the nBn detector (**Figure 13**) [84, 85] is essentially a photoconductor with unity gain, in which the junction (space charge region) is replaced by an electron blocking unipolar barrier (B) and the *p*-contact by an *n*-contact [8]. The wide bandgap undoped barrier layer is chosen to have minimal valence band offset [86]. Compared to the standard *p-i-n* design, detectors based on the nBn architecture have shown promise in suppressing currents associated with SRH centers, the GR component of dark current, and mesa lateral surface imperfections, thereby reducing the required temperature of operation [87, 88].

4.2.2. pBn design

In pBn structure devices, the *p-n* junction can either be located at the interface between the heavily doped *p*-type material and the lower doped barrier, or within the lower barrier itself [33]. This type of architecture is preferable when a large barrier in the conduction band offset is not achievable, allowing for zero bias operation [89].
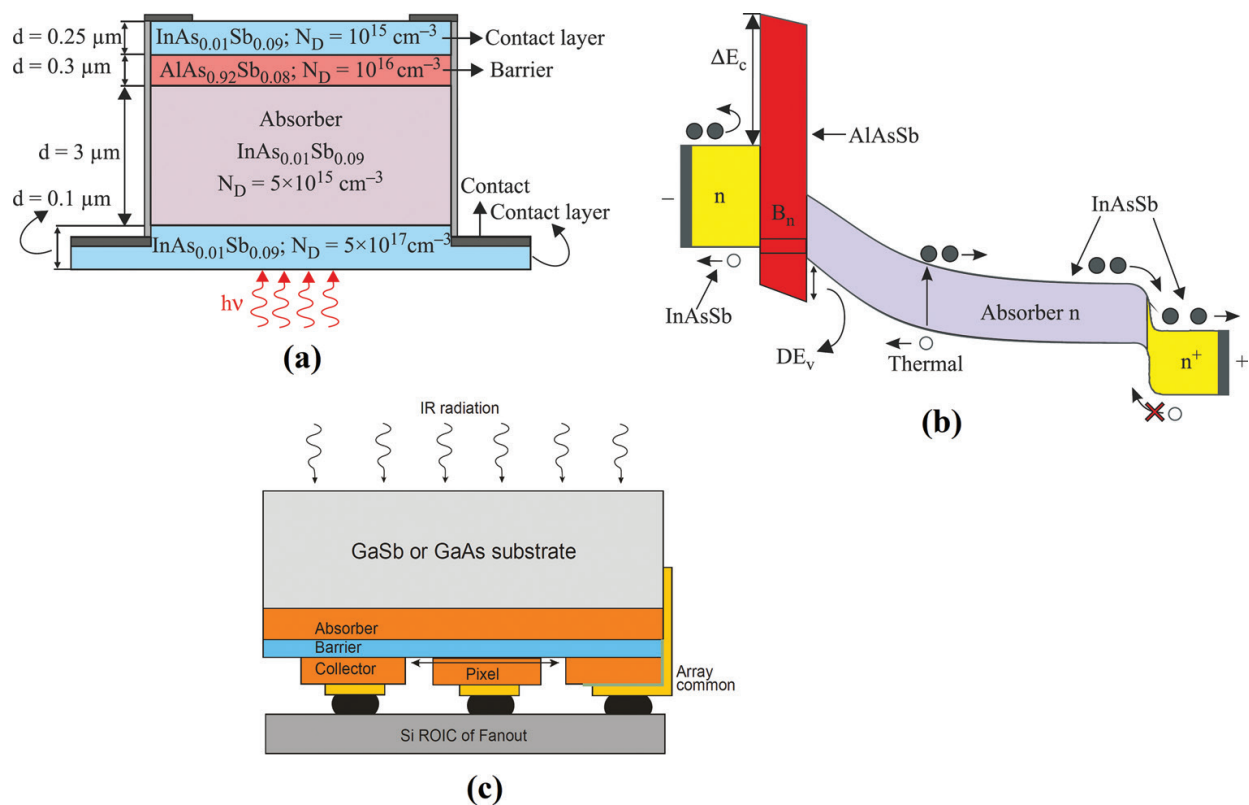
Figure 13. MWIR InAsSb/AlAsSb nBn SLS detector: (a) device structure, and (b) simulated energy band diagram under reverse bias conditions [84]; and (c) potential detector array (FPA) architecture [85].

4.2.3. pBp design

The pMp design consists of two *p*-doped superlattice active regions and a thin valence band barrier, producing electrical transport due to minority carriers (electrons) with low current density [22]. A large energy offset in the valence band prevents the movement of minority electrons but allows photogenerated majority carrier current to flow freely [29]. The higher mobility of electrons in comparison with holes in SLS pBp detectors results in greater photoresponse. The biasing requirements for SLS pBp detectors were demonstrated to be lower compared to those reported for nBn detectors [68, 79]. *D** and QE performance of MWIR and LWIR InAs/GaSb pBp detectors has been shown to be superior to that of comparable QWIP detectors, but somewhat inferior to the performance of MCT detectors operating over the same bands [90].

4.3. Supercell superlattices

Structures selectively designated as *supercell superlattices* are further variations of the unipolar barrier structure concept that constitute somewhat more complex designs than buried junction devices. Three primary varieties of supercell SLS architectures exist: M-, W-, and N-structures. As might be expected, these were named according to the similarities between the shapes of the respective letters and the band alignment of the constituent detector layers.

4.3.1. M-structure

M-structure detectors, originally developed for controlling BTB tunneling and consequently diffusion current for LWIR wavelengths, were subsequently found to accomplish this as well for the MWIR to allow increased active region doping levels [91]. The M-structure comprises a thin AlSb barrier inserted in the center of a GaSb layer in a type II binary InAs/GaSb superlattice [13]. The high bandgap AlSb layer effectively blocks the electron and hole dark currents, thereby improving the R_0A and *D** performance in type II InAs/GaSb LWIR photodiodes [92]. The large carrier effective mass associated with the InAs/GaSb material in M-structure detectors has been shown to provide more freedom in tuning the bandgap compared to other type II SLS designs [93].

Two variations of M-structure SLS devices are the pMp and p-π-M-n designs. These differ primarily in their usage of the M-structure barrier, which is employed to block hole majority carriers in the pMp architecture [94], while in p-π-M-n devices to suppress tunneling current [95].

The unipolar barrier pMp device concept, initially demonstrated for the VLWIR regime, was developed to reduce dark current due to BTB tunneling and GR contributions [54]. **Figure 14** shows the band structure and working principle of a pMp detector, along with key associated performance characteristics [22, 95]. Devices comprising the pMp architecture consist of two *p*-doped superlattice active regions and a thin valence band M-barrier having zero conduction band discontinuity with respect to the *p*-type active regions [79]. By using the M-structure SL as a barrier region, the band alignments can be experimentally controlled, allowing for efficient extraction of photocurrent under applied biases of less than 50 meV [22]. It has been demonstrated that the dark current in a pMp detector can be decreased by an order of magnitude by reducing the doping concentration in the contact layer [96].
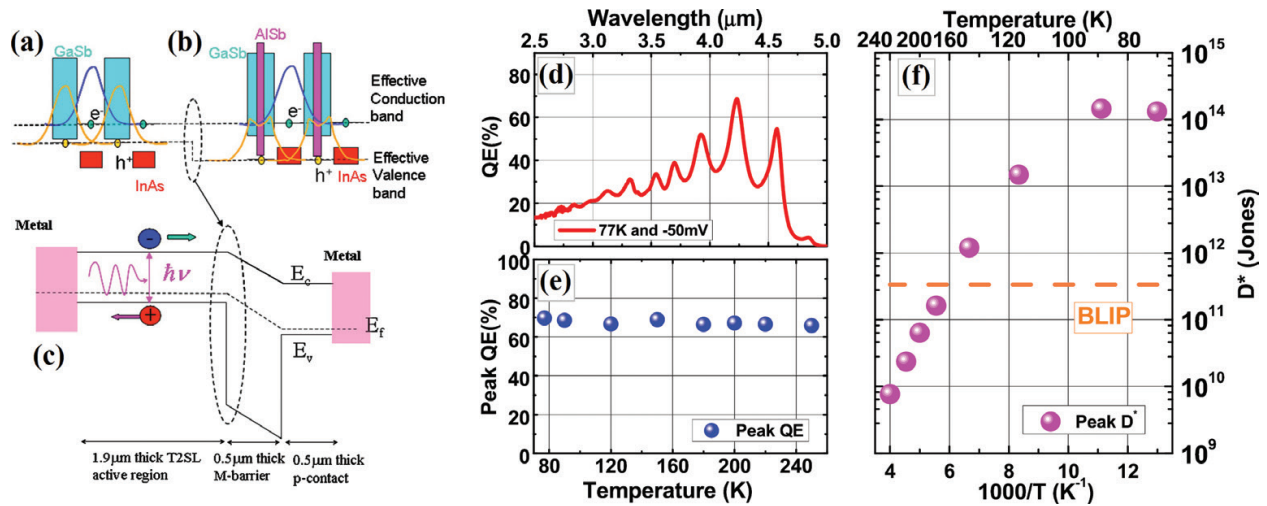
Figure 14. Band alignment and the creation of effective bandgap in (a) InAa/GaSb SL and (b) M-structure SL. (c) Schematic diagram and working principle of pMp design: the M-barrier blocks transport of majority holes, while allowing diffusion of minority electrons and photogenerated carriers from the active region [22]. (d) Quantum efficiency of photodetector at 77 K and −150 mV bias; (e) saturated QE at peak responsivity from 77 to 250 K; and (f) evolution of peak detectivity with temperature, where peak detectivity crosses calculated background-limited line at 165 K [95].

The p-π-M-n design consists of an M-barrier lightly n-doped to prevent excessive quantum efficiency bias dependence, inserted between the p and n regions of a standard p-π-n structure [8, 50]. In comparison with a basic p-π-n type design, the electric field in the depletion region of a p-π-M-n detector is reduced, and the tunneling barrier between the p and the n regions spatially broadened [95]. The first reported p-π-M-n detector which comprised a 500 nm M-barrier exhibited $R_0 A$ of 200 Ω cm^2 at 77 K, approximately one order of magnitude higher than that of a comparable p-π-n device without an M-layer barrier [94]. The dark current density J and $R_0 A$ versus bias voltage, and QE vs. wavelength, of a p-π-M-n detector are plotted in **Figure 15** [54]. Large format LWIR FPAs have been realized using for this architecture, one version of which demonstrated a QE of 78% and NETD of 23.6 mK at 81 K using 0.13 ms integration time [50].
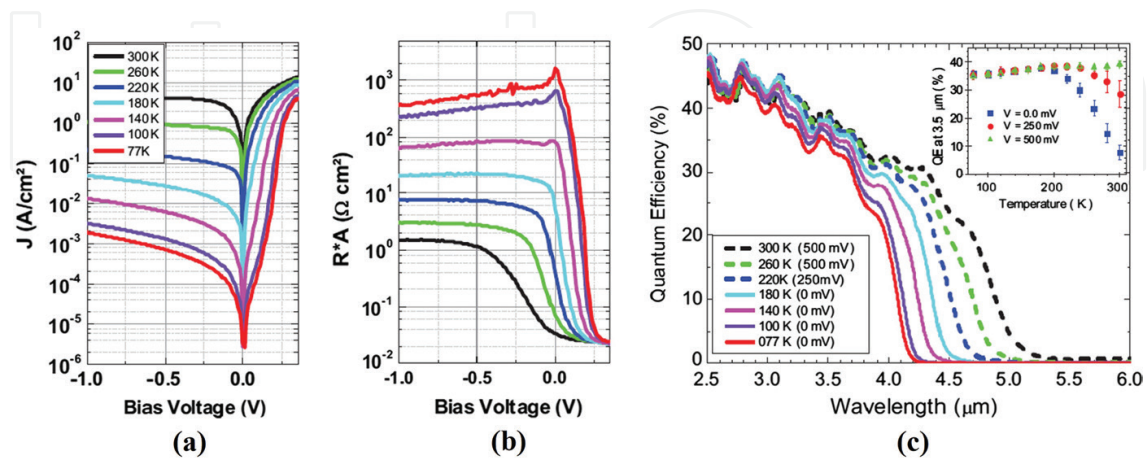
Figure 15. (a) Dark current density and (b) $R_0 A$ characteristics of a p-π-M-n SLS detector as a function of temperature. (c) Quantum efficiency spectra of the device at different operating temperatures, where inset shows temperature-dependent QE at a wavelength of 3.5 μm for different reverse biases [54].
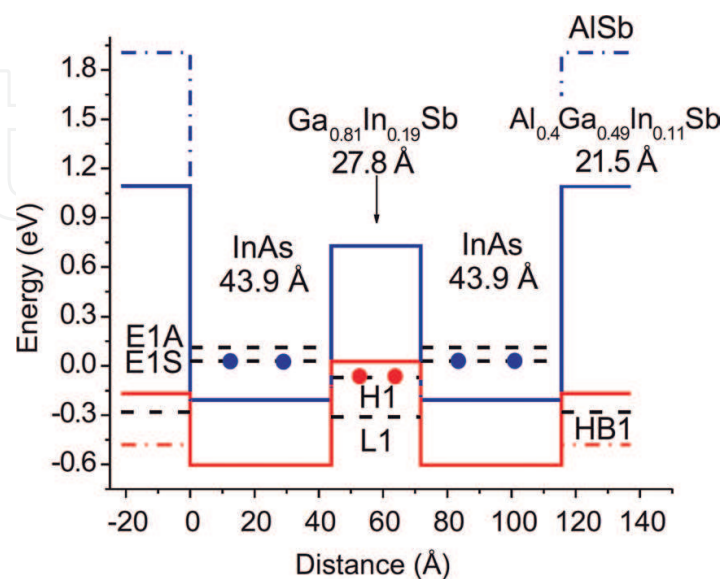
4.3.2. W-structure

The W-structured type-II SLS detector architecture reduces dark current due to strong suppression of BTB tunneling and GR processes [19]. Initially developed to increase the gain of MWIR lasers [13], it was reported to offer an order of magnitude improvement in dark current performance [12] and R_0A comparable to MCT. As illustrated in **Figure 16**, this type of design consists of InAs electron wells surrounding a GaInSb hole well and positioned between two quaternary AlGaInSb barriers [10]. The barriers enhance the electron–hole overlap while nearly localizing the wavefunctions, thereby increasing absorption near the band edge [80]. A subsequent generation W-structured LWIR detector was reported that employed a graded bandgap *p-i-n* structure and featured design improvements such as optimization to the barrier height that significantly increased minority carrier mobility and improved the quantum efficiency [97].

4.3.3. N-structure

The N-structure detector design consists of a *p-i-n* structure comprising two monolayer AlSb electron barriers inserted symmetrically between InAs and GaSb layers along the growth direction [8]. In this type of structure, the AlSb barrier pushes the electron and hole wavefunctions towards the layer edges under bias [98]. By improving the overlap of the spatially separated electron and hole wavefunctions, the absorption is increased while the dark current is reduced, enhancing the directivity [32].

4.4. Complementary barrier

A more sophisticated class of type II SLS structures contain complementary barriers that block both electron and holes, and are considered further variations of the double heterostructure design [99]. Two comparably designed representatives of this class were designated

Figure 16. Band profile of enhanced W-structure type II SLS photodiode [10].

complementary barrier infrared detector (*CBIRD*) by Ting et al. [23], and *pBiBn* by Gautam et al. [19]. These types of detectors have advantages in suppressing dark currents through blocking both majority and minority carriers, as well as circumventing technological problems arising from the need to make ohmic contacts with the widegap layers [100].

4.4.1. Complementary barrier infrared detector (CBIRD)

A CBIRD structure consists of a lightly doped *p*-type InAs/GaSb SL absorber surrounded by unipolar hole and electron blocking barriers [23]. As can be seen from **Figure 17(a)**, the electron barrier (eB) exists in the conduction band and the hole barrier (hB) in the valence band, where the two barriers complement one another to impede the flow of dark current [77]. A heavily doped *n*-type InAsSb layer adjacent to the eB SL acts as the bottom contact layer [9]. The barrier layers are designed to have approximately zero conduction band and valence band offsets with respect to the SL absorber. The absorber superlattice in CBIRD detectors is doped lightly *p*-type to improve the minority carrier (electron) mobility, and thus provide more favorable electron transport properties leading to enhanced performance including higher directivity [99]. **Figure 17(b)** plots the dark current density vs. applied bias for a CBIRD device [23].

4.4.2. pBiBn detector

The quantum-engineered pBiBn SLS detector structure [24] may be considered a hybrid between a conventional *p-i-n* structure and unipolar barrier concepts [101]. Like the CBIRD design, it was designed to mitigate the higher dark current in *p-n* junction and *p-i-n* photodetectors through incorporation of two unipolar carrier blocking barriers [18]. The first generation pBiBn detector demonstrated a significant improvement in performance over conventional *p-i-n* designs, with a fourfold increase in detectivity in the LWIR [24].

The band profile for a pBiBn design is shown in **Figure 18(a)**, and the detector layer structure given in **Figure 18(b)** [24, 101, 102]. It consists of an *n*-contact layer, followed by a hB layer, an
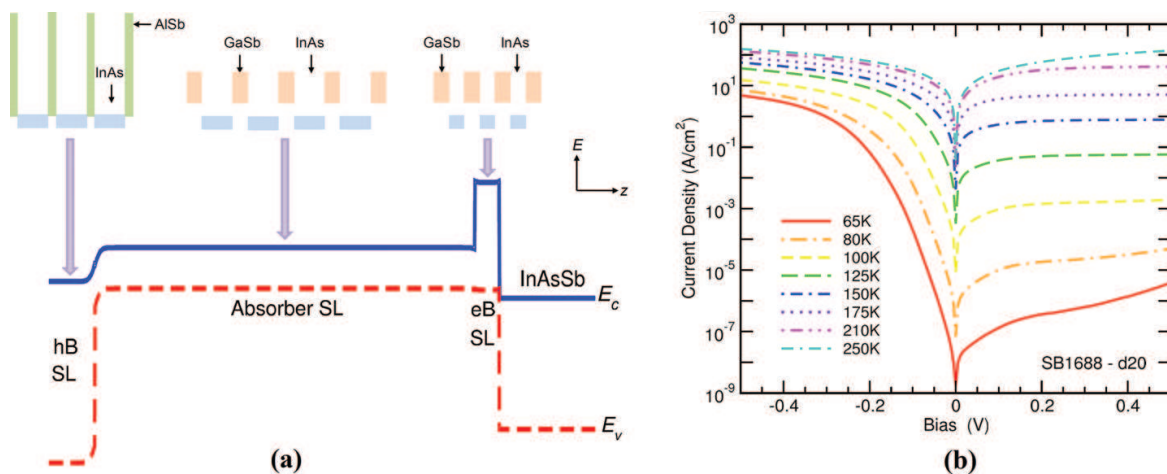

Figure 17. (a) Calculated zero-bias energy band diagram of a CBIRD structure, where a LWIR InAs/GaSb SL absorber is surrounded by an InAs/AlSb SL unipolar hB and shorter period eB [99]. (b) Dark current density as a function of applied bias for CBIRD detector, measured at various temperatures ranging from 65-250 K [23].
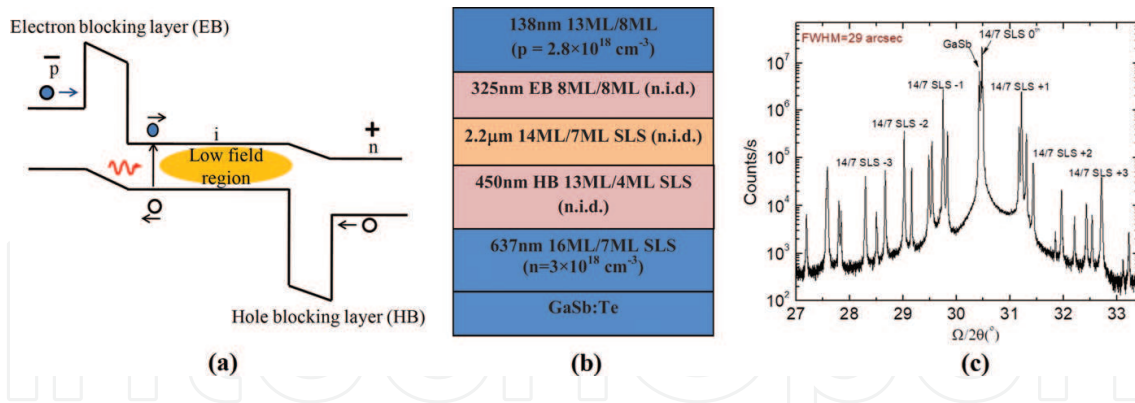
Figure 18. (a) Schematic drawing of band profile and (b) heterostructure schematic of pBiBn SLS detector [101, 102]. (c) XRD pattern of pBiBn material structure [24].

intrinsic absorber *i*-region, followed by an eB layer, and finally a *p*-contact layer. The unipolar carrier blocking layers (eB and hB) surrounding the type II InAs/GaSb SL absorber in the pBiBn structure comprises of heterojunctions with unique energy band alignments, for which the CBO ΔE_c for the eB layer (or VBO ΔE_v for the hB layer) is equivalent to the bandgap difference ΔE_g. The pBiBn band alignment and carrier transport differ from that in DH designs: instead of the electrons and holes being confined in the narrow bandgap material, a wider bandgap material with only a conduction band offset or a valence band offset is adopted. **Figure 18(c)** presents the X-ray diffraction (XRD) pattern from characterization of a pBiBn device [24].

The inclusion of hole and electron barriers flanking both sides of the absorber serves to lower diffusion currents by blocking the minority carriers from either side of the junction, while allowing unimpeded flow of photogenerated carriers. It also limits the voltage and substantially reduces the built-in electrical field in the absorber region [39]. This drop in electrical potential across the pBiBn active region is small compared to that in a conventional *pin* design because of
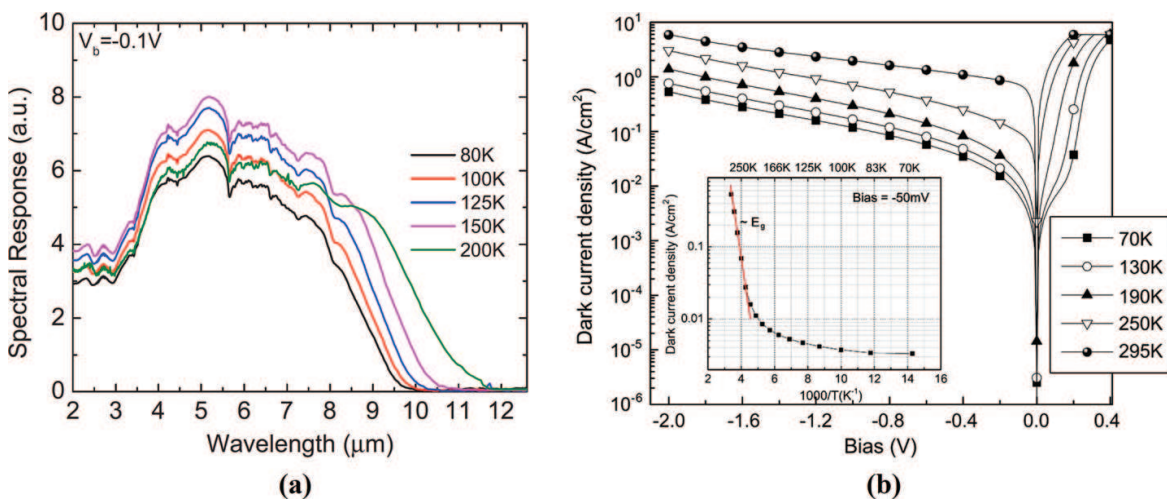
Figure 19. (a) Current–voltage (I-V) characteristics of type II SLS pBiBn detector; inset shows temperature dependent dark current density measured under applied bias of −50 mV [104]. (b) Measured spectral response for pBiBn detector as a function of temperature [102].

the eB and hB layers [103], which have wider bandgaps than the absorber region. The reduction of electric field within the absorber in the pBiBn structure effects a smaller depletion region, which further reduces the SRH dark current and suppresses TAT and BTB tunneling dark current components [24, 38]. **Figure 19(a)** and **(b)** plot I-V characteristics versus applied bias and spectral response vs. wavelength, respectively, for SLS pBiBn detectors [102, 104].

5. Type II SLS detectors: practical progress and trends

5.1. High operating temperature (HOT)

For advanced IR photodetectors and FPAs, high temperature operability is of great interest and in high demand for many applications. High operating temperature (HOT: ~150–300 K and above) capability enables significant advantages in cost, size, weight, and power (CSWaP) reduction resulting from the lessening of cooling load [105]. Initial efforts for developing HOT detectors concentrated on photoconductors and photoelectromagnetic (PEM) devices, material improvement to lower generation-recombination leakage mechanisms, alternate materials such as cascade devices, and SLS barrier structures such as nBn [106]. Type II MWIR SLS detectors and FPAs have certain advantages for HOT operation in relation to InSb, MCT, and QWIP devices, in many instances offering comparable performance at significantly higher operating temperatures [107].

Type II SLS detectors based on the InAs/GaSb/AlSb system have demonstrated HOT operation in both MWIR and LWIR regimes [38]. Achieving this typically requires minimizing the residual doping level in the intrinsic region, which is highly sensitive to crystal growth conditions [31]. **Figure 20(a)** compares images captured with a MWIR SLS FPA at different operating temperatures, and **Figure 20(b)** plots corresponding NETD versus temperature at different integration times [108, 109]. A MWIR pBiBn InAs/GaSb type II SLS was reported

(a)   (b)
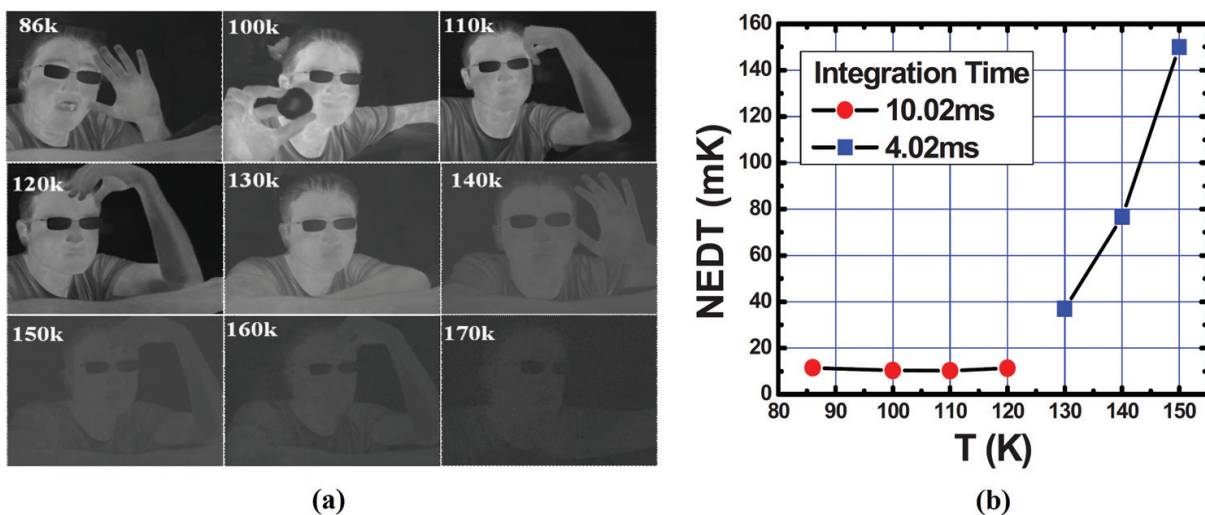
Figure 20. (a) MWIR images captured with type II SLS FPA over a range of temperatures [108]. (b) Corresponding NEDT measured at 86–150 K using *f*/2.3 optics [109].

that demonstrated operation up to 295 K, but the dark current density of the device was high and the spectral response relatively low, ruling out its practical use in detector applications at room temperature [38]. However, HOT nBn detectors were shown at 300 K to reach higher detectivities in comparison with standard InAsSb photodiodes [84, 110].

5.2. Large format FPAs

Recent improvements in the maturation of growth and fabrication process technologies, design of process tools and optics, reproducibility and yield, and spatial uniformity of final FPA devices have enabled and facilitated the transition to larger format FPAs [51, 111]. FPAs having resolutions up to 1024 × 1024 with pixel pitches 18 μm and smaller have been developed [48–51]. Large format, small pixel pitch FPAs clearly possess a number of benefits for IR imaging applications including larger fields of view and higher angular resolutions [77]. This is particularly advantageous for target tracking and surveillance applications, for example, by enabling longer detection ranges for a target tracking system with a fixed optical aperture [8].

A potential means of making the production of large format arrays more practical and commercially viable is to employ larger diameter substrate wafers. For example, only a single LWIR array with 18 μm pitch can be processed on a 2 in. diameter wafer, while one 3 in. wafer can allocate up to four such 1 k × 1 k arrays or one 2 k × 2 k array [113]. Consequently, in recent years there has been heightened demand for high performance material on non-native substrates that are cheaper and larger than GaSb despite significant (~7%) lattice mismatch [56]. **Figure 21** presents physical features [50] and a captured image [112] from a megapixel MWIR SLS FPA.

5.3. Multiband IR detection

Multiband (or multicolor) detectors are useful for various military and civil IR imaging applications involving identification of temperature differences and determination of thermal characteristics of objects, including remote sensing and target identification [37]. Multiband
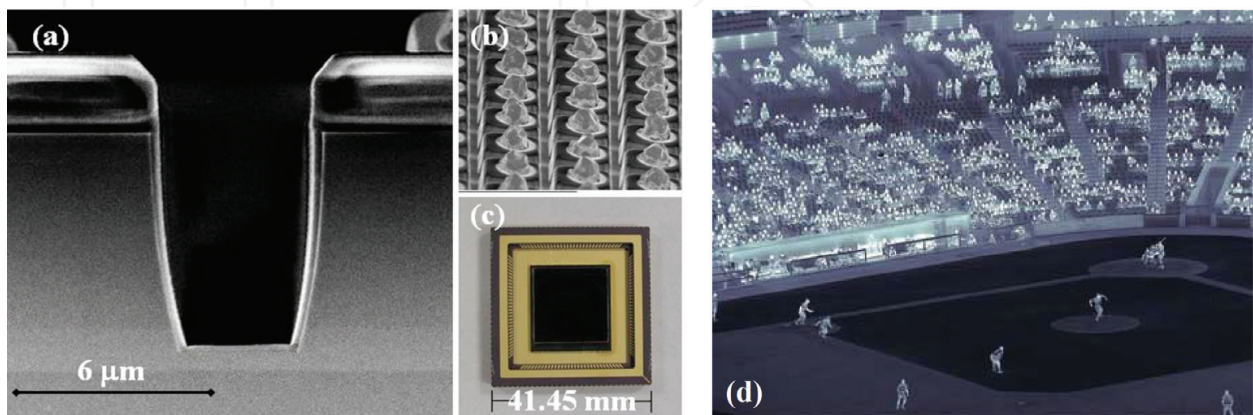
Figure 21. (a) Cross-sectional scanning electron micrograph of etched trench between two pixels in large format (1 k × 1 k) LWIR type II n-M-π-p SLS FPA; (b) FPA pixels with uniform indium bumps; and (c) FPA mounted on a chip carrier [50]. (d) Captured image of scene from baseball game using MWIR nBn FPA, also with 1 k × 1 k pixel resolution [112].

SLS photodetectors have been developed that combine wavelength bands from the SWIR to VLWIR. In addition, type II SLS multiband technology is compatible with commercially available ROICs, enabling development of many types of multiband SLS FPAs.

More conventional designs combining detection of MWIR and LWIR wavelength bands commonly consist of separate LWIR and MWIR superlattices separated by an AlGaSb unipolar barrier. Such MWIR/LWIR dual-band detectors typically possess pBp architectures comprising vertical designs based on two back-to-back InAs/GaSb SLS photodiodes separated by a common ground contact layer [90]. In such devices, properly biased unipolar barriers and thicker absorber regions block the migration of photogenerated carriers to reduce spectral crosstalk between the different absorber regions (channels) [100]. In multiband SLS detectors and FPAs, the selection of the desired band is typically achieved through alternating the polarity of the applied bias.

Successful fabrication of multiband SLS photodetectors requires the development of separate materials sensitive to each band, which necessitates prioritizing the optimization of the optical and electrical performance for each channel [114]. An advantage of type II SLS multiband detectors and FPAs compared to other technologies is relative design simplicity, while low hole mobility and limited lateral diffusion remain significant challenges [15].

Most multiband detectors and FPAs developed thus far are dual-band (i.e., dual-color). InAs/GaSb type II SLS FPAs with separate LWIR and MWIR absorbers have been developed with measured dark current densities in the low $\mu A/cm^2$ range and specific detectivities of up to 5×10^{11} Jones [30]. **Figure 22(a)** shows band diagrams for a dual-band MWIR/LWIR SLS pBp detector [115], and **Figure 22(b)** and **(c)** feature corresponding MWIR and LWIR images, respectively, from a dual-band detector demonstrating the contrast in appearance when imaging an optical filter [91].

Recent years have seen the development of various three-color SLS detector designs [52, 100, 116]. A MWIR/LWIR/VLWIR SLS detector has been reported within the past year in which the spectral crosstalk was reduced by controlling minority carrier transport through doping of the two active regions [116]. As seen in **Figure 23**, an innovative triple-band SWIR/
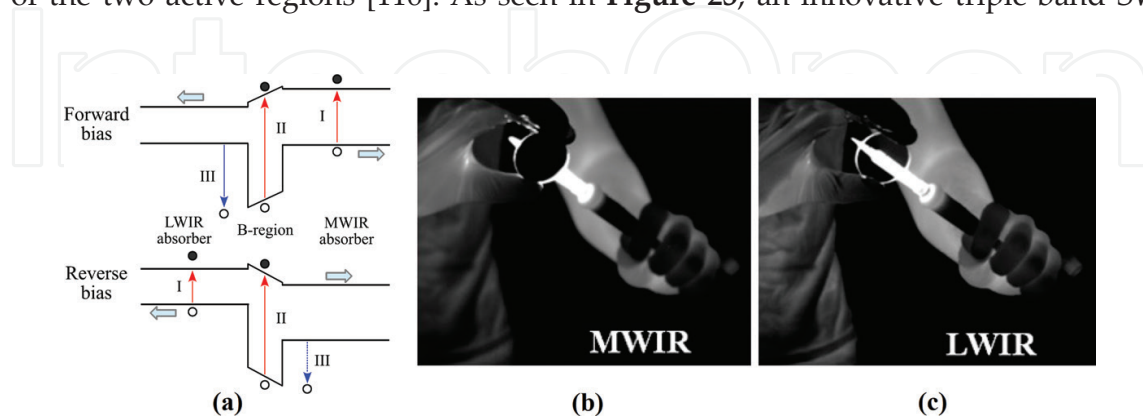
Figure 22. (a) Band alignment under forward and reverse biases for dual-band type II InAs/GaSb SLS photodetector based on a pBp architecture, showing effective optical transitions contributing to photocurrents (having dependence on the bias polarity) [115]. Images from (b) MWIR and (c) LWIR channels of dual-band FPA, capturing 11.3 μm narrow bandpass optical filter at 81 K [91].
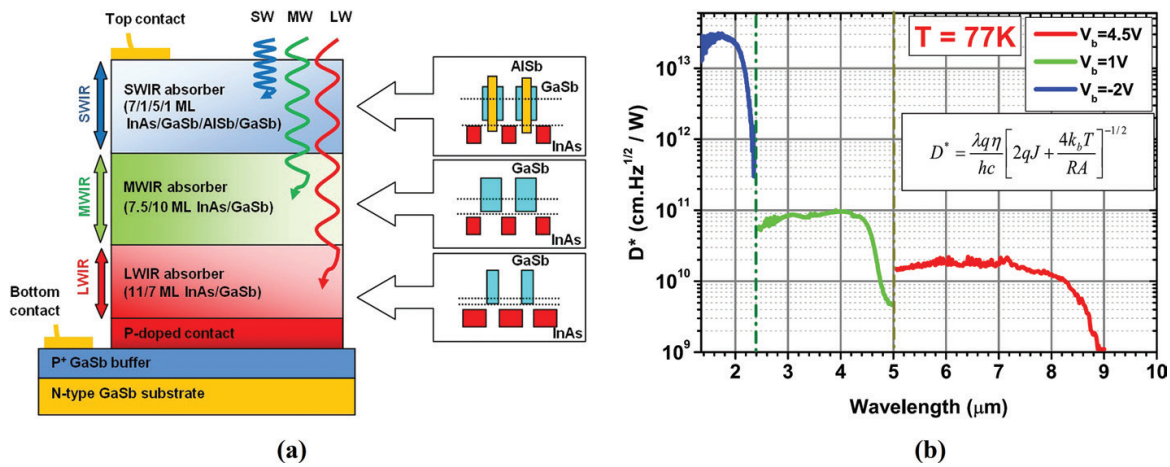
Figure 23. (a) Schematic diagram of triple-band SWIR/MWIR/LWIR photodiode structure with two terminal contacts and schematic band alignment of superlattices in three absorption layers. (b) Plotted directivities for the three channels at the wavelengths of interest at 77 K [52].

MWIR/LWIR device design was likewise reported recently, capable of sequentially performing as three individual single color photodetectors using only two terminals [52]. This device employed conduction band offsets and different doping levels between absorption layers to control the turn-on voltages for the individual channels.

5.4. High-speed imaging

The higher quantum efficiencies and reduced cooling requirements offered by type II SLS detectors and FPAs make them well suited for high frame rate applications with low integration times. InAs/GaSb SLS devices incorporate a potentially high-speed detector material in comparison to uncooled microbolometers, for which time constant constraints limit frame rates to under ~30 fps [110]. These properties make certain types of SLS detectors and FPAs
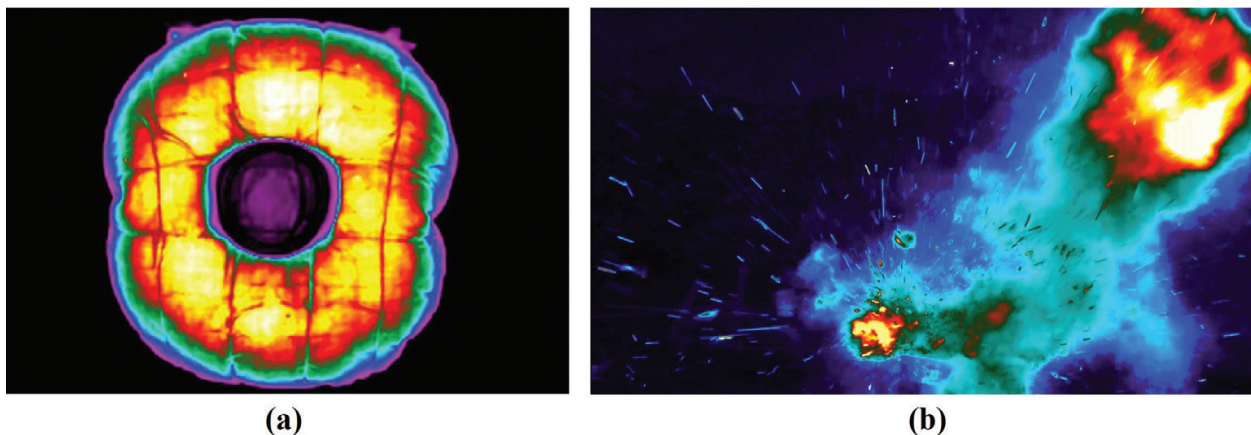
Figure 24. (a) Airbag deployment imaged by SLS camera with 160 μs integration time [58]. (b) Thermal image of munitions testing captured at 1000 fps and 640 × 512 resolution [117].

practical for detecting rapid temperature rises in concert with rapid scene motion, particularly at temperatures ~300 K and below [58].

While frame rates of 60 Hz are common for type II SLS detectors reported in recent years, for certain applications significantly higher capture speeds are required. Combined with new higher speed ROIC designs that are more linear across their entire dynamic range, SLS detectors can now accommodate integration times below 270 ns, providing frame rates of over 180 fps at 1028 × 1024 resolution, or over 1000 fps at 640 × 512 resolution [59, 117]. Such higher speed, faster frame rate detection capability has significant advantages in applications such as safety analysis and evaluation (**Figure 24(a)**) [58], ballistic and munitions testing (**Figure 24(b)**) [117], and missile seekers and missile warning systems [44].

6. Summary and conclusions

Type II superlattices possess a robustness and practical utility originating from the flexibility to control and manipulate the material system for practically any desired target of operability, while inheriting the benefits of mature III–V semiconductor growth and fabrication process technology [56]. The broad array of SLS detector/FPA architectures in existence today provides researchers with wide-ranging ability to control the various noise and dark current mechanisms to optimize SLS detector performance for electro-optical/IR applications. Progress and development in areas such as high temperature operability, multiband detection, and high-speed imaging have showcased some of the diverse and unique features of type II InAs/GaSb SLS devices. These have led to practical, real-world improvements in the field, many of which would not be possible using alternative IR detector technologies and material systems.

Type II SLS detectors and two dimensional FPAs based on the InAs/GaSb material system can theoretically provide higher performance than precedential IR detection technologies, including QWIP and HgCdTe detectors [28]. While in general type II SLS devices have yet to achieve such a noted benchmark, substantial progress in this area has been made and continues to be undertaken, as discussed in this Chapter. Further future progress and technical development in practical devices are still needed, potentially involving new discoveries and technological breakthroughs in material and structural engineering, for type II SLS to emerge as a leading technology. Nevertheless, these devices have had a definite and lasting impact the area of IR detection and imaging, and expectations are that type II SLS will remain a key enabling technology in the field for years and possibly decades to come.

Acknowledgements

(DARPA). The views, opinions and/or findings expressed are those of the author and should not be interpreted as representing the official views or policies of the Department of Defense or the U.S. Government.

Author details

Ashok K. Sood[1]*, John W. Zeller[1], Roger E. Welser[1], Yash R. Puri[1], Nibir K. Dhar[2], Priyalal S. Wijewarnasuriya[3] and Sanjay Krishna[4]

*Address all correspondence to: aksood@magnoliaoptical.com

1 Magnolia Optical Technologies, Woburn, MA, USA

2 U.S. Army Night Vision & Electronic Sensors Directorate, Fort Belvoir, VA, USA

3 U.S. Army Research Laboratory, Adelphi, MD, USA

4 Department of Electrical and Computer Engineering, Ohio State University, Columbus, OH, USA

References

[1] Pollehn H, Choi KK, Svensson S, Dhar N. IR material research at the Army Research Laboratory. In: Proceedings of SPIE, Infrared Technology and Applications XXXIII; 14 May 2007; Orlando, Florida. SPIE; 2007;**6542**:65420C. DOI: 10.1117/12.723659

[2] Martin TJ, Cohen MJ, Dries JC, Lange MJ. InGaAs/InP focal plane arrays for visible light imaging. In: Proceeding of SPIE, Infrared Technology and Applications XXX; 30 August 2004; Orlando, Florida. SPIE; 2004;**5406**: p. 39. DOI: 10.1117/12.542523

[3] Davis M, Devitt J, Greiner M, Rawe R, Timlin A, Wade D. Advanced FPA technology development at CMC electronics. In: Proceedings of SPIE, Infrared Systems and Photoelectronic Technology; 2-6 August 2004; Denver, Colorado. SPIE; 2004;**5563**: p. 63. DOI: 10.1117/12.565665

[4] Norton PW, Kohin M, Dovidio M, Becker B. Commercialization of uncooled infrared technology. In: Proceedings of SPIE, Infrared Systems and Photoelectronic Technology; 21 October 2004; Denver, Colorado. SPIE; 2004. p. 55-61. DOI: 10.1117/12.565663

[5] Myers S, Plis E, Khoshakhlagh A, Kim HS, Sharma Y, Dawson R, Krishna S, Gin A. The effect of absorber doping on electrical and optical properties of nBn based type-II InAs/GaSb strained layer superlattice infrared detectors. Applied Physics Letters. 2009;**95**:121110. DOI: 10.1063/1.3230069

[6] Tidrow MZ. Type II strained layer superlattice: A potential future IR solution. Infrared Physics & Technology. 2009;**52**:322-325. DOI: 10.1016/j.infrared.2009.05.028

[7] Plis EA. InAs/GaSb type-II superlattice detectors. Advances in Electronics. 2014;**2014**:1-12. DOI: 10.1155/2014/246769

[8] Martyniuk P, Antoszewski J, Martyniuk M, Faraone L, Rogalski A. New concepts in infrared photodetector designs. Applied Physics Reviews. 2014;**1**:041102. DOI: 10.1063/1.4896193

[9] Rogalski A. History of infrared detectors. Opto-Electronics Review. 2012;**20**:279-308. DOI: 10.2478/s11772-012-0037-7

[10] Rogalski A, Antoszewski J, Faraone L. Third-generation infrared photodetector arrays. Journal of Applied Physics. 2009;**105**:091101. DOI: 10.1063/1.3099572

[11] Rogalski A, Kopytko M, Martyniuk P. InAs/GaSb type-II superlattice infrared detectors: three decades of development. In: Proceedings of SPIE, Infrared Technology and Applications XLIII; 3 May 2017; Anaheim, California. SPIE; 2017;**10177**: p. 1017715. DOI: 10.1117/12.2272817

[12] Rogalski A. Material considerations for third generation infrared photon detectors. Infrared Physics & Technology. 2007;**50**:240-252. DOI: 10.1016/j.infrared.2006.10.015

[13] Aifer EH, Tischler JG, Warner JH, Vurgaftman I, Kim JC, Meyer JR, Bennett BR, Whitman LJ, Jackson EM, Lorentzen JR. W-structured type-II superlattice based long and very-long wavelength infrared photodiodes. In: Proceedings of SPIE, Quantum Sensing and Nanophotonic Devices II; 25 March 2005; San Jose, California. SPIE; 2005;**5732**:259-272. DOI: 10.1117/12.597134

[14] Plis EA, Kutty MN, Krishna S. Passivation techniques for InAs/GaSb strained layer superlattice detectors. Laser & Photonics Reviews. 2013;**7**:45-59. DOI: 10.1002/lpor.201100029

[15] Haugan HJ, Olson BV, Brown GJ, Kadlec EA, Kim JK, Shaner EA. Significantly enhanced carrier lifetimes of very long-wave infrared absorbers based on strained-layer InAs/GaInSb superlattices. Optical Engineering. 2017;**56**:091604. DOI: 10.1117/1.OE.56.9.091604

[16] Rogalski A. Competitive technologies of third generation infrared photon detectors. Opto-electronics Review. 2006;**14**:84-98. DOI: 10.2478/s11772-006-0012-2

[17] Rodriguez JB, Plis E, Bishop G, Sharma YD, Kim H, Dawson LR, Krishna S. nBn structure based on InAs/GaSb type-II strained layer superlattices. Applied Physics Letters. 2007;**91**:043514. DOI: 10.1063/1.2760153

[18] Treider LA, Morath CP, Cowan VM, Tian ZB, Krishna S. Radiometric characterization of an LWIR, type-II strained layer superlattice pBiBn photodetector. Infrared Physics & Technology. 2015;**70**:70-75. DOI: 10.1016/j.infrared.2014.09.043

[19] Vurgaftman I, Aifer EH, Canedy CL, Tischler JG, Meyer JR, Warner JH, Jackson EM, Hildebrandt G, Sullivan GJ. Graded band gap for dark-current suppression in long-wave infrared W-structured type-II superlattice. Applied Physics Letters. 2006;**89**:121114. DOI: 10.1063/1.2356697

[20] Maimon S, Wicks GW. nBn detector, an infrared detector with reduced dark current and higher operating temperature. Applied Physics Letters. 2006;**89**:151109. DOI: 10.1063/1.2360235

[21] Nguyen BM, Razeghi M, Nathan V, Brown GJ. Type-II M structure photodiodes: an alternative material design for mid-wave to long wavelength infrared regimes. In: Proceedings of SPIE, Quantum Sensing and Nanophotonic Devices IV; 12 February 2007; San Jose, California. SPIE; 2007;**6479**: p. 64790S. DOI: 10.1117/12.711588

[22] Nguyen BM, Bogdanov S, Pour SA, Razeghi M. Minority electron unipolar photodetectors based on type II InAs/GaSb/AlSb superlattices for very long wavelength infrared detection. Applied Physics Letters. 2009;**95**:183502. DOI: 10.1063/1.3258489

[23] Ting DZY, Hill CJ, Soibel A, Keo SA, Mumolo JM, Nguyen J, Gunapala SD. A high-performance long wavelength superlattice complementary barrier infrared detector. Applied Physics Letters. 2009;**95**:023508. DOI: 10.1063/1.3177333

[24] Gautam N, Kim HS, Kutty MN, Plis E, Dawson LR, Krishna S. Performance improvement of longwave infrared photodetector based on type-II InAs/GaSb superlattices using unipolar current blocking layers. Applied Physics Letters. 2010;**96**:231107. DOI: 10.1063/1.3446967

[25] Tian Z, Hinkey RT, Yang RQ, Qiu Y, Lubyshev D, Fastenau JM, Liu AWK, Johnson MB. Interband cascade infrared photodetectors with enhanced electron barriers and p-type superlattice absorbers. Journal of Applied Physics. 2012;**111**:024510. DOI: 10.1063/1.3678003

[26] Yang RQ, Tian Z, Cai Z, Klem JF, Johnson MB, Liu HC. Interband cascade infrared photodetectors with superlattice absorbers. Journal of Applied Physics. 2010;**107**:054514. DOI: 10.1063/1.3327415

[27] Martyniuk P, Rogalski A. Quantum-dot infrared photodetectors: Status and outlook. Progress in Quantum Electronics. 2008;**32**:89-120. DOI: 10.1016/j.pquantelec.2008.07.001

[28] Rhiger DR. Performance comparison of long-wavelength infrared type II superlattice devices with HgCdTe. Journal of Electronic Materials. 2011;**40**:1815-1822. DOI: 10.1007/s11664-011-1653-6

[29] Plis E, Myers S, Ramirez D, Smith EP, Rhiger D, Chen C, Phillips JD, Krishna S. Dual color longwave InAs/GaSb type-II strained layer superlattice detectors. Infrared Physics & Technology. 2015;**70**:93-98. DOI: 10.1016/j.infrared.2014.09.027

[30] Plis E, Naydenkov M, Myers S, Klein B, Gautam N, Krishna SS, Smith EP, Johnson S, Krishna S. Dual-band pBp detectors based on InAs/GaSb strained layer superlattices. Infrared Physics & Technology. 2013;**59**:28-31. DOI: 10.1016/j.infrared.2012.12.005

[31] Li JV, Hill CJ, Mumolo J, Gunapala S, Mou S, Chuang SL. Midinfrared type-II InAs/GaSb superlattice photodiodes toward room temperature operation. Applied Physics Letters. 2008;**93**:163505. DOI: 10.1063/1.2949744

[32] Salihoglu O, Muti A, Kutluer K, Tansel T, Turan R, Ergun Y, Aydinli A. "N" structure for type-II superlattice photodetectors. Applied Physics Letters. 2012;**101**:073505. DOI: 10.1063/1.4745841

[33] Hood AD, Evans AJ, Ikhlassi A, Lee DL, Tennant WE. LWIR strained-layer superlattice materials and devices at Teledyne imaging sensors. Journal of Electronic Materials. 2010;**39**:1001-1006. DOI: 10.1007/s11664-010-1091-x

[34] Esaki L, Tsu R. Superlattice and negative differential conductivity in semiconductors. IBM Journal of Research and Development. 1970;**14**:61-65. DOI: 10.1147/rd.141.0061

[35] Sai-Halasz GA, Tsu R, Esaki L. A new semiconductor superlattice. Applied Physics Letters. 1977;**30**:651-653. DOI: 10.1063/1.89273

[36] Smith DL, Mailhiot C. Proposal for strained type II superlattice infrared detectors. Journal of Applied Physics. 1987;**62**:2545-2548. DOI: 10.1063/1.339468

[37] Fuchs F, Weimer U, Pletschen W, Schmitz J, Ahlswede E, Walther M, Wagner J, Koidl P. High performance InAs/Ga$_{1-x}$In$_x$Sb superlattice infrared photodiodes. Applied Physics Letters. 1997;**71**:3251-3253. DOI: 10.1063/1.120551

[38] Gautam N, Myers S, Barve AV, Klein B, Smith EP, Rhiger D, Plis E, Kutty MN, Henry N, Schuler-Sandy T, Krishna S. Band engineered HOT midwave infrared detectors based on type-II InAs/GaSb strained layer superlattices. Infrared Physics & Technology. 2013;**59**:72-77. DOI: 10.1016/j.infrared.2012.12.017

[39] DeCuir EA, Meissner GP, Wijewarnasuriya PS, Gautam N, Krishna S, Dhar NK, Welser RE, Sood AK. Long-wave type-II superlattice detectors with unipolar electron and hole barriers. Optical Engineering. 2012;**51**:124001. DOI: 10.1117/1.OE.51.12.124001

[40] Zhou X, Li D, Huang J, Zhang Y, Mu Y, Ma W, Tie X, Zuo D. Mid-wavelength type II InAs/GaSb superlattice infrared focal plane arrays. Infrared Physics & Technology. 2016;**78**:263-267. DOI: 10.1016/j.infrared.2016.08.014

[41] Rogalski A. Recent progress in infrared detector technologies. Infrared Physics & Technology. 2011;**54**:136-154. DOI: 10.1016/j.infrared.2010.12.003

[42] Zheng L, Tidrow M, Aitcheson L, O'Connor J, Brown S. Developing high-performance III–V superlattice IRFPAs for defense: challenges and solutions. Proceedings of SPIE, Infrared Technology and Applications XXXVI; 23 April 2010; Orlando, Florida. SPIE; 2010;**7660**: p. 76601E. DOI: 10.1117/12.852239

[43] Haddadi A, Chen G, Chevallier R, Hoang AM, Razeghi M. InAs/InAs$_{1-x}$Sb$_x$ type-II superlattices for high performance long wavelength infrared detection. Applied Physics Letters. 2014;**105**:121104. DOI: 10.1063/1.4896271

[44] Cabanski W, Münzberg M, Rode W, Wendler J, Ziegler J, Fleißner J, Fuchs F, Rehm R, Schmitz J, Schneider H, Walther M. Third-generation focal plane array IR detection modules and applications. In: Proceedings of SPIE, Infrared Technology and Applications XXX; 30 August 2004. Orlando, Florida. SPIE; 2005;**5406**:184-192. DOI: 10.1117/12.542186

[45] Razeghi M, Delaunay PY, Nguyen BM, Hood A, Hoffman D, McClintock R, Wei Y, Michel E, Nathan V, Tidrow MZ. First demonstration of ~10 microns FPAs in InAs/GaSb SLS. In: Digest of the LEOS Summer Topical Meetings; 7-19 July 2006; Quebec City, Que., Canada. New York: IEEE; 2006. p. 20. DOI: 10.1109/LEOSST.2006.1694049

[46] Münzberg M, Breiter R, Cabanski W, Lutz H, Wendler J, Ziegler J, Rehm R, Walther M. Multi spectral IR detection modules and applications. In: Proceedings of SPIE, Infrared Technology and Applications XXXII; 5 May 2006; Orlando (Kissimmee), Florida. SPIE; 2006;**6206**: p. 620627. DOI: 10.1117/12.665467

[47] Hill CJ, Soibel A, Keo SA, Mumolo JM, Ting DZ, Gunapala SD, Rhiger DR, Kvaas RE, Harris SF. Demonstration of mid-and long-wavelength infrared antimonide-based focal plane arrays. In: Proceedings of SPIE, Infrared Technology and Applications XXXV; 7 April 2009; Orlando, Florida. SPIE; 2009;**7298**: p. 729804. DOI: 10.1117/12.818692

[48] Gunapala SD, Ting DZ, Hill CJ, Nguyen J, Soibel A, Rafol SB, Keo SA, Mumolo JM, Lee MC, Liu JK, Yang B. Demonstration of a 1024 × 1024 pixel InAs-GaSb superlattice focal plane array. IEEE Photonics Technology Letters. 2010;**22**:1856-1858. DOI: 10.1109/LPT.2010.2089677

[49] Haddadi A, Ramezani-Darvish S, Chen G, Hoang AM, Nguyen BM, Razeghi M. High operability 1024 × 1024 long wavelength type-II superlattice focal plane array. IEEE Journal of Quantum Electronics. 2012;**48**:221-228. DOI: 10.1109/JQE.2011.2175903

[50] Manurkar P, Ramezani-Darvish S, Nguyen BM, Razeghi M, Hubbs J. High performance long wavelength infrared mega-pixel focal plane array based on type-II superlattices. Applied Physics Letters. 2010;**97**:193505. DOI: 10.1063/1.3514244

[51] Klipstein PC, Avnon E, Azulai D, Benny Y, Fraenkel R, Glozman A, Hojman E, Klin O, Krasovitsky L, Langof L, Lukomsky I. Type II superlattice technology for LWIR detectors. In: Proceedings of SPIE, Infrared Technology and Applications XLII; 20 May 2016; Baltimore, Maryland. SPIE; 2016;**9819**: p. 98190T. DOI: 10.1117/12.2222776

[52] Hoang AM, Dehzangi A, Adhikary S, Razeghi M. High performance bias-selectable three-color short-wave/mid-wave/long-wave infrared photodetectors based on type-II InAs/GaSb/AlSb superlattices. Scientific Reports. 2016;**6**:24144. DOI: 10.1038/srep24144

[53] Haddadi A, Suo XV, Adhikary S, Dianat P, Chevallier R, Hoang AM, Razeghi M. High-performance short-wavelength infrared photodetectors based on type-II InAs/$InAs_{1-x}Sb_x$/$AlAs_{1-x}Sb_x$ superlattices. Applied Physics Letters. 2015;**107**:141104. DOI: 10.1063/1.4932518

[54] Razeghi M, Haddadi A, Hoang AM, Huang EK, Chen G, Bogdanov S, Darvish SR, Callewaert F, McClintock R. Advances in antimonide-based type-II superlattices for infrared detection and imaging at center for quantum devices. Infrared Physics & Technology. 2013;**59**:41-52. DOI: 10.1016/j.infrared.2012.12.008

[55] Sood AK, Zeller JW, Richwine RA, Puri YR, Efstathiadis H, Haldar P, Dhar NK, Polla DL. SiGe based visible-NIR photodetector technology for optoelectronic applications. In: Yasin M, Arof H, Harum SW, editors. Advances in Optical Fiber Technology: Fundamental Optical Phenomena and Applications. Rijeka: InTech; 2015. p. 315-351. DOI: 10.5772/59065

[56] Razeghi M, Nguyen BM. Advances in mid-infrared detection and imaging: A key issues review. Reports on Progress in Physics. 2014;**77**:082401. DOI: 10.1088/0034-4885/77/8/082401

[57] Martyniuk P, Rogalski A. Performance comparison of barrier detectors and HgCdTe photodiodes. Optical Engineering. 2014;**53**:106105. DOI: 10.1117/1.OE.53.10.106105

[58] Richards A. Advantages of strained-layer superlattice detectors for high-speed thermal events. In: Proceedings of SPIE, Quantum Sensing and Nano Electronics and Photonics XIV; 27 January 2017; San Francisco, California. SPIE; 2017;**10111**: p. 101111B. DOI: 10.1117/12.2250039

[59] Bainter C, High-speed IR. Detectors aid ballistic testing. Photonics Spectra. 2017;**51**:63-67

[60] Klein B. Defect investigations in InAs/GaSb type-II strained layer superlattice [thesis]. Albuquerque: The University of New Mexico; 2014

[61] Salvetti O, Ronchi LA, Corsi C, Rogalski A, Strojnik M. Advanced infrared technology and applications. Advances in Optical Technologies. 2013;**2013**:1-2. DOI: 10.1155/2013/459074

[62] Rogalski A. Progress in focal plane array technologies. Progress in Quantum Electronics. 2012;**36**:342-473. DOI: 10.1016/j.pquantelec.2012.07.001

[63] Hood A, Razeghi M, Aifer EH, Brown GJ. On the performance and surface passivation of type II InAs/ GaSb superlattice photodiodes for the very-long-wavelength infrared. Applied Physics Letters. 2005;**87**:151113. DOI: 10.1063/1.2089170

[64] Han X, Xiang W, Hao HY, Jiang DW, Sun YY, Wang GW, Xu YQ, Niu ZC. Very long wavelength infrared focal plane arrays with 50% cutoff wavelength based on type-II InAs/GaSb superlattice. Chinese Physics B. 2017;**26**:018505. DOI: 10.1088/1674-1056/26/1/018505

[65] Hoang AM, Chen G, Chevallier R, Haddadi A, Razeghi M. High performance photodiodes based on InAs/InAsSb type-II superlattices for very long wavelength infrared detection. Applied Physics Letters. 2014;**104**:251105. DOI: 10.1063/1.4884947

[66] Wei Y, Gin A, Razeghi M, Brown GJ. Advanced InAs/GaSb superlattice photovoltaic detectors for very long wavelength infrared applications. Applied Physics Letters. 2002;**80**:3262-3264. DOI: 10.1063/1.1476395

[67] Li X, Jiang D, Zhang Y, Zhao L. Interface optimization and fabrication of InAs/GaSb type II superlattice for very long wavelength infrared photodetectors. Superlattices and Microstructures. 2016;**91**:238-243. DOI: 10.1016/j.spmi.2016.01.013

[68] Das S, Das U, Gautam N, Krishna S. Type-II InAs/GaSb photodiode array pixel isolation by femto-second laser anneal. Infrared Physics & Technology. 2016;**78**:162-166. DOI: 10.1016/j.infrared.2016.07.023

[69] Chakrabarti P, Gawarikar A, Mehta V, Garg D. Effect of trap-assisted tunneling (TAT) on the performance of homojunction mid-infrared photodetectors based on InAsSb. Journal of Microwaves, Optoelectronics and Electromagnetic Applications. 2006;**5**:1-4

[70] Rhiger DR, Kvaas RE, Harris SF, Hill CJ. Characterization of LWIR diodes on InAs/GaSb type-II superlattice material. Infrared Physics & Technology. 2009;**52**:304-309. DOI: 10.1016/j.infrared.2009.05.009

[71] Grein CH, Garland J, Flatte ME. Strained and unstrained layer superlattices for infrared detection. Journal of Electronic Materials. 2009;**38**:1800-1804. DOI: 10.1007/s11664-009-0757-8

[72] Cervera C, Jaworowicz K, Aït-Kaci H, Chaghi R, Rodriguez JB, Ribet-Mohamed I, Christol P. Temperature dependence performances of InAs/GaSb superlattice photodiode. Infrared Physics & Technology. 2011;**54**:258-262. DOI: 10.1016/j.infrared.2010.12.025

[73] Yang QK, Fuchs F, Schmitz J, Pletschen W. Investigation of trap-assisted tunneling current in InAs/(GaIn) Sb superlattice long-wavelength photodiodes. Applied Physics Letters. 2002;**81**:4757-4759. DOI: 10.1063/1.1529306

[74] Asplund C, von Würtemberg RM, Lantz D, Malm H, Martijn H, Plis E, Gautam N, Krishna S. Performance of mid-wave T2SL detectors with heterojunction barriers. Infrared Physics & Technology. 2013;**59**:22-27. DOI: 10.1016/j.infrared.2012.12.004

[75] Sah CT, Noyce RN, Shockley W. Carrier generation and recombination in pn junctions and pn junction characteristics. In: Proceedings of the IRE, September 1957. New York: IEEE; 1957;**45**:1228-1243. DOI: 10.1109/JRPROC.1957.278528

[76] Nguyen J, Ting DZ, Hill CJ, Soibel A, Keo SA, Gunapala SD. Dark current analysis of InAs/GaSb superlattices at low temperatures. Infrared Physics & Technology. 2009;**52**:317-321. DOI: 10.1016/j.infrared.2009.05.022

[77] Plis E, Kutty MN, Myers S, Kim HS, Gautam N, Dawson LR, Krishna S. Passivation of long-wave infrared InAs/GaSb strained layer superlattice detectors. Infrared Physics & Technology. 2011;**54**:252-257. DOI: 10.1016/j.infrared.2010.12.024

[78] Kim HS, Plis E, Gautam N, Myers S, Sharma Y, Dawson LR, Krishna S. Reduction of surface leakage current in InAs/GaSb strained layer long wavelength superlattice detectors using SU-8 passivation. Applied Physics Letters. 2010;**97**:143512. DOI: 10.1063/1.3499290

[79] Martyniuk P, Kopytko M, Rogalski A. Barrier infrared detectors. Opto-Electronics Review. 2014;**22**:127-146. DOI: 10.2478/s11772-014-0187-x

[80] Johnson JL, Samoska LA, Gossard AC, Merz JL, Jack MD, Chapman GR, Baumgratz BA, Kosai K, Johnson SM. Electrical and optical properties of infrared photodiodes using the InAs/Ga$_{1-x}$In$_x$ Sb superlattice in heterojunctions with GaSb. Journal of Applied Physics. 1996;**80**:1116-1127. DOI: 10.1063/1.362849

[81] Canedy CL, Aifer EH, Warner JH, Vurgaftman I, Jackson EM, Tischler JG, Powell SP, Olver K, Meyer JR, Tennant WE. Controlling dark current in type-II superlattice photodiodes. Infrared Physics & Technology. 2009;**52**:326-334. DOI: 10.1016/j.infrared.2009.09.004

[82] Aifer EH, Maximenko SI, Yakes MK, Yi C, Canedy CL, Vurgaftman I, Jackson EM, Nolde JA, Affouda CA, Gonzalez M, Meyer JR, Clark KP, Pinsukanjana PR. Recent developments

in type-II superlattice-based infrared detectors. In: Proceedings of SPIE, Infrared Technology and Applications XXXVI; 4 May 2010; Orlando, Florida. SPIE; 2010;**7660**: p. 76601Q. DOI: 10.1117/12.855028

[83] Myers S, Plis E, Morath C, Cowan V, Gautam N, Klein B, Kutty MN, Naydenkov M, Sandy TS, Krishna S. Comparison of superlattice based dual color nBn and pBp infrared detectors. In: Proceedings of SPIE, Infrared Sensors, Devices, and Applications, and Single Photon Imaging II; 17 September 2011; San Diego, California. SPIE; 2011;**8155**: p. 815507. DOI: 10.1117/12.894986

[84] Martyniuk P, Rogalski A. Theoretical modeling of InAsSb/AlAsSb barrier detectors for higher-operation-temperature conditions. Optical Engineering. 2014;**53**:017106. DOI: 10.1117/1.OE.53.1.01710

[85] Rogalski A, Martyniuk P, Kopytko M. Challenges of small-pixel infrared detectors: A review. Reports on Progress in Physics. 2016;**79**:046501. DOI: 10.1088/0034-4885/79/4/046501

[86] Kim HS, Plis E, Rodriguez JB, Bishop GD, Sharma YD, Dawson LR, Krishna S, Bundas J, Cook R, Burrows D, Dennis R. Mid-IR focal plane array based on type-II InAs/GaSb strain layer superlattice detector with nBn design. Applied Physics Letters. 2008;**92**:183502. DOI: 10.1063/1.2920764

[87] Khoshakhlagh A, Rodriguez JB, Plis E, Bishop GD, Sharma YD, Kim HS, Dawson LR, Krishna S. Bias dependent dual band response from InAs/Ga(in)Sb type II strain layer superlattice detectors. Applied Physics Letters. 2007;**91**:263504. DOI: 10.1063/1.2824819

[88] Klein B, Plis E, Kutty MN, Gautam N, Albrecht A, Myers S, Krishna S. Varshni parameters for InAs/GaSb strained layer superlattice infrared photodetectors. Journal of Physics D: Applied Physics. 2011;**44**:075102. DOI: 10.1088/0022-3727/44/7/075102

[89] Martyniuk P, Gawron W, Rogalski A. Theoretical modeling of HOT HgCdTe barrier detectors for the mid-wave infrared range. Journal of Electronic Materials. 2013;**42**:3309-3319. DOI: 10.1007/s11664-013-2737-2

[90] Plis EA, Krishna SS, Gautam N, Myers S, Krishna S. Bias switchable dual-band InAs/GaSb superlattice detector with pBp architecture. IEEE Photonics Journal. 2011;**3**:234-240. DOI: 10.1109/JPHOT.2011.2125949

[91] Razeghi M, Haddadi A, Hoang AM, Chen G, Ramezani-Darvish S, Bijjam P. High performance bias-selectable dual-band mid−/long-wavelength infrared photodetectors and focal plane arrays based on InAs/GaSb type-II superlattices. In: Proceedings of SPIE, Infrared Technology and Applications XXXIX; 11 June 2013; Baltimore, Maryland. SPIE; 2013;**8704**: p. 87040S. DOI: 10.1117/12.2019147

[92] Delaunay PY, Nguyen BM, Hoffman D, Huang EK, Razeghi M. Background limited performance of long wavelength infrared focal plane arrays fabricated from M-structure InAs-GaSb superlattices. IEEE Journal of Quantum Electronics. 2009;**45**:157-162. DOI: 10.1109/JQE.2008.2002667

[93] Hoang AM, Chen G, Haddadi A, Abdollahi Pour S, Razeghi M. Demonstration of shortwavelength infrared photodiodes based on type-II InAs/GaSb/AlSb superlattices. Applied Physics Letters. 2012;**100**:211101. DOI: 10.1063/1.4720094

[94] Nguyen BM, Hoffman D, Delaunay PY, Razeghi M. Dark current suppression in type II InAs/GaSb superlattice long wavelength infrared photodiodes with M-structure barrier. Applied Physics Letters. 2007;**91**:163511. DOI: 10.1063/1.2800808

[95] Chen G, Haddadi A, Hoang AM, Chevallier R, Razeghi M. Demonstration of type-II superlattice MWIR minority carrier unipolar imager for high operation temperature application. Optics Letters. 2015;**40**:45-47. DOI: 10.1364/OL.40.000045

[96] Nguyen BM, Chen G, Hoang AM, Abdollahi Pour S, Bogdanov S, Razeghi M. Effect of contact doping in superlattice-based minority carrier unipolar detectors. Applied Physics Letters. 2011;**99**:033501. DOI: 10.1063/1.3613927

[97] Aifer EH, Tischler JG, Warner JH, Vurgaftman I, Bewley WW, Meyer JR, Kim JC, Whitman LJ, Canedy CL, Jackson EM. W-structured type-II superlattice long-wave infrared photodiodes with high quantum efficiency. Applied Physics Letters. 2006;**89**:053519. DOI: 10.1063/1.2335509

[98] Salihoglu O, Hostut M, Tansel T, Kutluer K, Kilic A, Alyoruk M, Sevik C, Turan R, Ergun Y, Aydinli A. Electronic and optical properties of 4.2 μm "N" structured superlattice MWIR photodetectors. Infrared Physics & Technology. 2013;**59**:36-40. DOI: 10.1016/j.infrared.2012.12.007

[99] Ting DZ, Soibel A, Nguyen J, Höglund L, Khoshakhlagh A, Rafol B, Keo SA, Liao A, Mumolo JM, Liu JK, Gunapala SD. Type II superlattice barrier infrared detector. In: Proceedings of SPIE, Infrared Remote Sensing and Instrumentation XIX; 17 September 2011; San Diego, California. SPIE; 2011;**8154**: p. 81540L. DOI: 10.1117/12.896240

[100] Gautam N, Naydenkov M, Myers S, Barve AV, Plis E, Rotter T, Dawson LR, Krishna S. Three color infrared detector using InAs/GaSb superlattices with unipolar barriers. Applied Physics Letters. 2011;**98**:121106. DOI: 10.1063/1.3570687

[101] Tian Z, DeCuir EA, Wijewarnasuriya PS, Pattison JW, Gautam N, Krishna S, Dhar N, Welser RE, Sood AK. Low-dark current structures for long-wavelength type-II strained layer superlattice photodiodes. In: Proceedings of SPIE, Infrared Technology and Applications XXXIX; 11 June 2013; Baltimore, Maryland. SPIE; 2013;**8704**: p. 870415. DOI: 10.1117/12.2015489

[102] Gautam N, Myers S, Barve AV, Klein B, Smith EP, Rhiger DR, Kim HS, Tian ZB, Krishna S. Barrier engineered infrared photodetectors based on type-II InAs/GaSb strained layer superlattices. IEEE Journal of Quantum Electronics. 2013;**49**:211-217. DOI: 10.1109/JQE.2012.2236643

[103] Klipstein P. "XBn" barrier photodetectors for high sensitivity and high operating temperature infrared sensors. In: Proceedings of SPIE, Infrared Technology and

Applications XXXIV; 23 April 2008; Orlando, Florida. SPIE; 2008;**6940**: p. 69402U. DOI: 10.1117/12.778848

[104] Plis E, Klein B, Myers S, Gautam N, Smith EP, Krishna S. High operating temperature midwave infrared InAs/GaSb superlattice photodetectors on (111) GaSb substrates. IEEE Electron Device Letters. 2013;**34**:426-428. DOI: 10.1109/LED.2012.2236534

[105] Ariyawansa G, Reyner CJ, Steenbergen EH, Duran JM, Reding JD, Scheihing JE, Bourassa HR, Liang BL, Huffaker DL. InGaAs/InAsSb strained layer superlattices for mid-wave infrared detectors. Applied Physics Letters. 2016;**108**:022106. DOI: 10.1063/1.4939904

[106] Pusz W, Kowalewski A, Martyniuk P, Gawron W, Plis E, Krishna S, Rogalski A. Mid-wavelength infrared type-II InAs/GaSb superlattice interband cascade photodetectors. Optical Engineering. 2014;**53**:043107. DOI: 10.1117/1.OE.53.4.043107

[107] Delaunay PY, Razeghi M. Noise analysis in type-II InAs/GaSb focal plane arrays. Journal of Applied Physics. 2009;**106**:063110. DOI: 10.1063/1.3224958

[108] Razeghi M, Abdollahi Pour S, Huang E, Chen G, Haddadi A, Nguyen B. Type-II InAs/GaSb photodiodes and focal plane arrays aimed at high operating temperatures. Opto-Electronics Review. 2011;**19**:261-269. DOI: 10.2478/s11772-011-0028-0

[109] Pour SA, Huang EW, Chen G, Haddadi A, Nguyen BM, Razeghi M. High operating temperature midwave infrared photodiodes and focal plane arrays based on type-II InAs/GaSb superlattices. Applied Physics Letters. 2011;**98**:143501. DOI: 10.1063/1.3573867

[110] Wei Y, Hood A, Yau H, Gin A, Razeghi M, Tidrow MZ, Nathan V. Uncooled operation of type-II InAs/GaSb superlattice photodiodes in the midwavelength infrared range. Applied Physics Letters. 2005;**86**:233106. DOI: 10.1063/1.1947908

[111] Gautam N, Myers S, Barve AV, Klein B, Smith EP, Rhiger DR, Dawson LR, Krishna S. High operating temperature interband cascade midwave infrared detector based on type-II InAs/GaSb strained layer superlattice. Applied Physics Letters. 2012;**101**:021106. DOI: 10.1063/1.4733660

[112] Adams A, Rittenberg E. HOT IR sensors improve IR camera size, weight, and power. Laser Focus World. 2014;**50**:83-87

[113] Nguyen BM, Chen G, Hoang MA, Razeghi M. Growth and characterization of long-wavelength infrared type-II superlattice photodiodes on a 3-in GaSb wafer. IEEE Journal of Quantum Electronics. 2011;**47**:686-690. DOI: 10.1109/JQE.2010.2103049

[114] Hoang AM, Chen G, Haddadi A, Razeghi M. Demonstration of high performance bias-selectable dual-band short–/mid-wavelength infrared photodetectors based on type-II InAs/GaSb/AlSb superlattices. Applied Physics Letters. 2013;**102**:011108. DOI: 10.1063/1.4720094

[115] Lao YF, Pitigala PK, Unil Perera AG, Plis E, Krishna SS, Wijewarnasuriya PS. Band offsets and carrier dynamics of type-II InAs/GaSb superlattice photodetectors studied by

internal photoemission spectroscopy. Applied Physics Letters. 2013;**103**:181110. DOI: 10.1063/1.4827881

[116] Jiang DW, Xiang W, Guo FY, Hao HY, Han X, Li XC, Wang GW, Xu YQ, Yu QJ, Niu ZC. Low crosstalk three-color infrared detector by controlling the minority carriers type of InAs/GaSb superlattices for middle-long and very-long wavelength. Chinese Physics Letters. 2016;**33**:048502. DOI: doi.org/10.1088/0256-307X/33/4/048502

[117] Smith M. FLIR X6900sc Camera Captures Temperature Images at 1,000 Frames per Second [Internet]. 2016. Available from: http://www.industrytap.com/flir-x6900sc-camera-captures-temperature-images-at-1000-frames-per-second/35359 [Accessed: Jul 15, 2017]